Article

Preclinical In Vitro Studies with 3D Spheroids to Evaluate Cu(DDC)$_2$ Containing Liposomes for the Treatment of Neuroblastoma

Friederike Hartwig *[ID], **Monika Köll-Weber and Regine Süss**

Department of Pharmaceutical Technology and Biopharmacy, Institute of Pharmaceutical Sciences, University of Freiburg, Sonnenstr. 5, 79104 Freiburg, Germany; monika.koell-weber@pharmazie.uni-freiburg.de (M.K.-W.); regine.suess@pharmazie.uni-freiburg.de (R.S.)
* Correspondence: fri.ha@hotmail.de

Abstract: Preclinical in vitro studies of drug candidates for anticancer therapy are generally conducted on well-established 2D cell models. Unfortunately, these models are unable to mimic the properties of in vivo tumors. However, in vitro 3D models (spheroids) have been proven to be superior in reflecting the tumor microenvironment. Diethyldithiocarbamate (DDC$^-$) is the active metabolite of Disulfiram, an approved drug for alcoholism and repurposed for cancer treatment. DDC$^-$ binds copper in a molar ratio of 2:1 resulting in a water-insoluble Cu(DDC)$_2$ complex exhibiting anticancer activities. Delivery of the Cu(DDC)$_2$ complex using nanoparticulate carriers provides decisive advantages for a parental application. In this study, an injectable liposomal Cu(DDC)$_2$ formulation was developed and the toxicity was compared with a 2D neuroblastoma and a 3D neuroblastoma cell model. Our results indicate that Cu(DDC)$_2$ liposomes complied with the size requirements of nanoparticles for intravenous injection and demonstrated high drug to lipid ratios as well as colloidal stability upon storage. Furthermore, an efficient cytotoxic effect on neuroblastoma 2D cell cultures and a very promising and even more pronounced effect on 3D cell cultures in terms of neuroblastoma monoculture and neuroblastoma co-culture with primary cell lines was proven, highly encouraging the use of Cu(DDC)$_2$ liposomes for anticancer therapy.

Keywords: Disulfiram; Cu(DDC)$_2$; liposomes; drug delivery; storage stability; neuroblastoma; 3D spheroids

1. Introduction

The development of drug candidates for anticancer therapy needs proper preclinical in vitro and in vivo studies to prevent clinical trial failure. The assessment of drug potency and selectiveness is of particular importance. The drug candidate should be able to reach the target tissue and eliminate cancer cells without significantly affecting non-malignant cells [1]. Regarding in vitro assays, 2D cell monoculture models are most frequently used. These models are easily established, generate reproducible results, and are performable at low costs. They can be applied as a primary testing model using cancer cells, as well as non-malignant cells to assess efficiency, toxicity, and selectiveness of anticancer drugs. However, 2D cell monoculture models are unable to reflect the properties of in vivo tumors and their resistance to drugs [2]. Performing in vitro tests with 2D models unfortunately often leads to false positive testing results and, when being further examined in preclinical steps, to ineffective treatment of tumor xenografts. As an alternative, in vitro multicellular 3D models more accurately represent the microenvironment of in vivo tumors, e.g., allowing cells to secrete extracellular matrix (ECM) components. Cells can interact with the ECM and among each other, affecting cell proliferation, differentiation, gene and protein expression, and resistance to anticancer drugs [3]. 3D cultures can be categorized as scaffold-free or scaffold-based culture systems, where scaffolds can be produced with natural or synthetic

material. Scaffold-free systems are often referred to as spheroids [4]. Similar to solid tumors, spheroids display different cell layers building gradients of nutrients, oxygen, and waste. The outer layer consists of highly proliferating cells, the middle layer of quiescent cells and the core, depending on the spheroid size, of necrotic cells [5]. The cellular arrangement and the diffusional limit to mass transport form barriers for drugs and nanoparticles, e.g., liposomes [6,7]. Size, charge, and surface characteristics of nanoparticles can influence electrostatic interactions with the ECM and therefore penetration and uptake into the spheroid [8].

This study combines the evaluation of a novel anticancer drug delivery system and its effectivity in 2D and 3D cell models. Diethyldithiocarbamate (DDC^-) is described to be the active metabolite of Disulfiram (DSF) and is able to chelate Cu^{2+} in a 2:1 molar ratio resulting in a water insoluble $Cu(DDC)_2$ complex, which exhibits anticancer activity [8,9]. DSF, which was approved in 1951 for anti-alcoholism medication, came into focus for anticancer studies where it was shown, that the anticancer activity of DSF, which is rapidly reduced to its active metabolite DDC^-, strongly depends on the presence of Cu^{2+} [10]. Anyhow, co-administration of DSF and Cu^{2+} results in very low in vivo concentrations of $Cu(DDC)_2$, due to poor in vivo stability and rapid degradation of DSF in the presence of serum [8]. The administration of preformed $Cu(DDC)_2$ is expected to enhance anticancer effects. However, the poor aqueous solubility of $Cu(DDC)_2$, and consequently the insufficient bioavailability results in only low efficiency in preclinical models. Wehbe et al. (2016) published a method to circumvent solubility problems of $Cu(DDC)_2$ by using liposomes as nanoscale reaction vessels [8]. Liposomes containing Cu^{2+} in the aqueous core are loaded with DDC^-, which is able to diffuse through the lipid bilayer. Inside the aqueous core, DDC^- chelates Cu^{2+} and precipitates as $Cu(DDC)_2$. In this study, the liposome preparation method described by Wehbe et al. (2016) was used with modified purification steps and the introduction of surface area filtration to remove non-encapsulated $Cu(DDC)_2$ from $Cu(DDC)_2$ liposomes [8]. Non-PEGylated and PEGylated $Cu(DDC)_2$ liposomes with a liposomal composition of DSPC:Chol [55:45 molar ratio] and DSPC:Chol:DSPE-mPEG$_{2000}$ [50:45:5 molar ratio] were analyzed for colloidal stability, drug release during storage and cytotoxicity in 2D and 3D cell models. For the latter, an easy-handling and low-cost method was used to generate reproducible spheroids as a sophisticated primary in vitro testing model for anticancer drugs. Therefore, spheroids were cultivated as 3D cancer cell monocultures or 3D co-cultures with primary human cells. Comparative cell experiments were performed with cancer and primary human cell 2D monocultures. Neuroblastoma cells (LS) [11] were used as cancer cell line, which appeared to be highly suitable for spheroid formation.

Neuroblastoma is the most common pediatric extra-cranial solid tumor and accounts for approximately 15% of all cancer-related deaths in infants and children [12–14]. Acquiring multidrug resistance is a major obstacle to the successful treatment of neuroblastoma [15,16]. In addition to the administration of multi-chemotherapy regimens to overcome drug resistance, alternative approaches have been explored. Inhibiting the potency of cancer stem cells (CSCs), which are key drivers of tumor progression, metastasis, and drug resistance, is of particular importance [15,17]. It was shown, that aldehyde dehydrogenases (ALDH) are important key players to maintain the role of CSCs [17], which includes inhibitors of ALDH as potential candidates for new therapeutic approaches. Recent studies show effective inhibition of ALDH through DSF as well as $Cu(DDC)_2$ treatment [18–21]. In this context, $Cu(DDC)_2$ is highlighted as a potential candidate. The use of a liposomal and parenterally injectable $Cu(DDC)_2$-formulation is expected to be an alternative approach for the treatment of neuroblastoma in comparison to multi-chemotherapy regimens. Cytotoxic effects of a liposomal $Cu(DDC)_2$-formulation are evaluated with in vitro neuroblastoma 3D spheroids. This 3D in vitro system suggests a more appropriate cell model that significantly better simulates the physiological conditions of a tumor as compared to a 2D cell model.

2. Materials and Methods

2.1. Materials

1,2-distearoyl-sn-glycero-3-phosphocholine (DSPC) and 1,2-distearoyl-sn-glycero-3-phosphoethanolamine-N-[methoxy(polyethylene glycerol)-2000] (DSPE-mPEG$_{2000}$) were generously donated by Lipoid GmbH (Ludwigshafen, Germany). Cholesterol and 3,3′-dioctadecyloxacarbocyanin perchlorate (DiO, catalog number 42364) were purchased from Sigma Aldrich (Darmstadt, Germany). RPMI 1640 with (cat. no. P04-18500) and without (catalog number P04-16520) phenol red, DMEM (catalog number P04-04500), sodium pyruvate 10 nM, PBS w/o Ca^{2+} and Mg^{2+}, Trypsin/EDTA 0.05%/0.02% and 0.25%/0.02% were obtained from PAN Biotech (Aidenbach, Germany). Fetal calf serum (FCS) was purchased from Sigma Aldrich. Sephadex G-50 was obtained from GE Healthcare Life Science (Marlborough, MA, USA), CellTiter Glo® 2D and 3D assays (catalog number G7572 and G9683) from Promega (Walldorf, Germany), calcein-AM (catalog number C3099) from Molecular Probes (Eugene, OR, USA), and propidium iodide (PI, catalog number CN74.1) from Carl Roth (Karlsruhe, Germany). Copper sulphate, HEPES, sodium diethyldithiocarbamate trihydrate, sucrose, and all other chemicals were purchased from Carl Roth (Germany). Vivaspin Turbo 4, filtration unit, 100,000 MWCO (catalog number VSO4T42) was purchased from Sartorius and sterile cellulose acetate filter, 0.2 μm and 0.45 μm from VWR (International, Radnor, PA, USA).

2.2. Liposomal Preparation

The preparation of Cu(DDC)$_2$ liposomes followed the idea of Wehbe et al. (2016) and was modified as indicated (Figure 1) [8]. Liposomes composed of DSPC:Chol [55:45 molar ratio] and DSPC:Chol:DSPE-mPEG$_{2000}$ [50:45:5 molar ratio] were prepared by the thin film hydration method [22] with subsequent hand extrusion [23]. Briefly, organic stock solutions were transferred at the indicated ratios into a round bottom flask and the solvent was removed via rotary evaporation. The flask was placed under vacuum for at least 2 h to remove residual solvent. The lipid film was hydrated with 1 mL of an aqueous CuSO$_4$ solution (Cu^{2+}, 150 mM in aqua destillata, pH 3.5) resulting in a lipid concentration of 40 mM. After 30 min of swelling and agitation, the formed liposomes were extruded for 41 passages through a polycarbonate membrane with a pore diameter of 80 nm (Nuclepore®, GE Healthcare Life Science, Chicago, IL, USA). Solvent removal, film hydration, and extrusion were performed at 65 °C which is 10 °C above the phase transition temperature of DSPC. Prior to the addition of DDC$^-$, Cu^{2+} liposomes were separated from non-encapsulated Cu^{2+} via size exclusion chromatography (SEC). The SEC column, prepared with Sephadex G-50, was equilibrated with an EDTA containing sucrose buffer (SHE, 300 mM sucrose, 20 mM HEPES, 30 mM EDTA, pH 7.4). Hereafter, buffer exchange with an EDTA-free sucrose buffer (SH, 300 mM sucrose, 20 mM HEPES, pH 7.4) was performed via three centrifugation steps at room temperature (RT) and 3000× *g* for 1 h using Vivaspin® Turbo 4 filtration units (100 kDa MWCO, Sartorius, Germany). To allow the diffusion of DDC$^-$ into the liposomal interior, followed by complexation of DDC$^-$ with the liposomal encapsulated Cu^{2+}, the preparation was left at 25 °C for 10 min at 300 rpm in a shaker. Free DDC$^-$ was removed via filtration units as described above with the final SH formulation buffer. The resulting Cu(DDC)$_2$ liposomes were prefiltered via a cellulose acetate (CA) 0.45 μm filter (VWR International, USA) to remove non-incorporated and precipitated Cu(DDC)$_2$. For cell experiments, the liposomes were sterile filtered under aseptic conditions through a 0.2-μm CA filter. Fluorescent-labeled liposomes (with 0.5% DiO, related to the total lipid amount) were used to perform flow cytometry experiments. For the DiO liposome preparation, DiO was added from an organic stock solution to the residual liposomal components in a round bottom flask. The lipid film was treated as described above. In this case, the lipid film was hydrated with 1 mL HEPES buffered saline (HBS, 10 mM HEPES, 140 mM NaCl, pH 7.4), resulting in a final lipid concentration of 20 mM. The liposomal dispersion was extruded through an 80-nm polycarbonate membrane (Nuclepore®, GE Healthcare Life

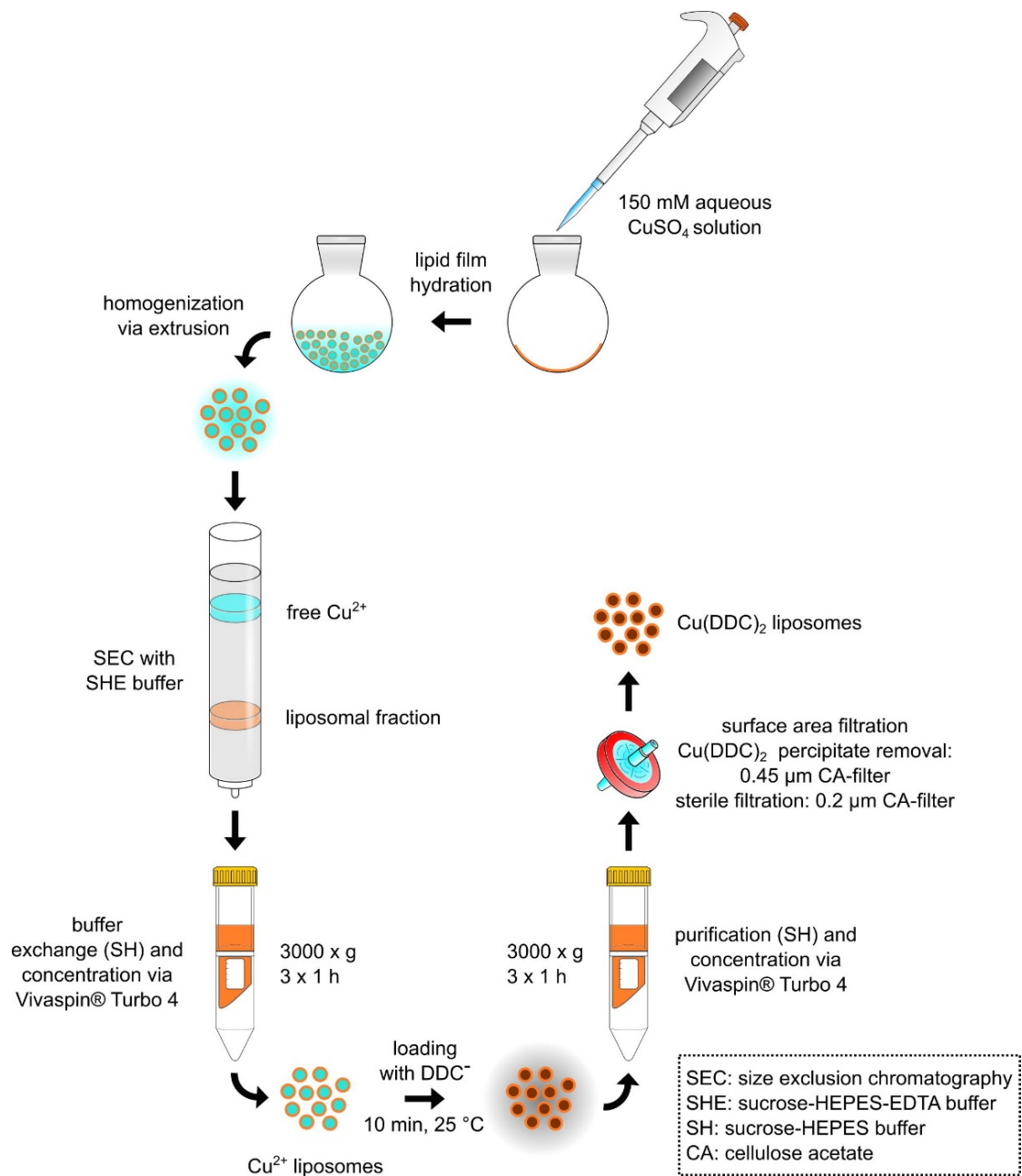Science, USA) after 30 min of swelling and agitation and stored at 4–6 °C protected from light until use.

Figure 1. Schematic representation of Cu(DDC)$_2$ liposome preparation by generating Cu^{2+} liposomes followed by remote loading of DDC$^-$. This method was modified from Wehbe et al. (2016) [8].

2.3. Surface Area Filtration

The usage of surface area filtration had to be validated to remove non-incorporated and precipitated Cu(DDC)$_2$ from liposomal Cu(DDC)$_2$. For this purpose, freshly prepared Cu(DDC)$_2$ liposomes were prefiltered through a 0.45-μm CA filter and sterile-filtered through a 0.2-μm CA filter. These filtration steps are part of the liposomal production process and are referred to as the 1st + 2nd filtrations. To validate the influence of filtration steps on liposomal stability, two additional filtration steps were performed referred to as the 3rd and 4th filtrations. Filtered samples were taken after each filtration step for analyzing lipid and Cu(DDC)$_2$ content.

2.4. Quantification of Lipids and Cu(DDC)$_2$

The Cu(DDC)$_2$ liposomes were analyzed for total lipid and Cu(DDC)$_2$ content. Phospholipid content was determined via Bartlett assay [24] and Cu(DDC)$_2$ content via a spectrophotometric method. Quantification of DDC$^-$ was determined by measuring the absorbance of complexed Cu^{2+} at a wavelength of λ_{max} = 435 nm with a GENESYS 10S UV-Vis spectrophotometer (Thermo Scientific™, Waltham, MA, USA). Standards were prepared by mixing Cu^{2+} solutions (0.015–0.1 µmol Cu^{2+} in aqua dest., pH 3.5) with a 70-µmol methanolic DDC$^-$ stock solution resulting in the formation of solubilized Cu(DDC)$_2$. The calibration curve was obtained by plotting the absorbance versus the amount of substance of Cu^{2+}. DDC$^-$ chelates Cu^{2+} in a 2:1 molar ratio and, therefore, the amount of complexed DDC$^-$ can be calculated. For the analysis of Cu(DDC)$_2$ liposomes, the use of methanol has the advantage of disrupting the liposomal membrane and solubilizing the liposomal trapped Cu(DDC)$_2$. Subsequently, the absorbance of complex Cu^{2+} and accordingly the amount of Cu(DDC)$_2$ can be determined via UV-Vis spectrometry. Linearity was verified by linear least square regression analysis, where y is the absorbance, x the amount of substance of sample, m the slope, and b the y intercept:

$$y = mx + b \tag{1}$$

In this study, the Cu(DDC)$_2$ concentrations of Cu(DDC)$_2$ liposomes refer to the amount of intraliposomal complexed DDC$^-$, calculated as described above. Accordingly, the drug concentration should be indicated with DDC$^-$/Cu^{2+}, whereby the molar ratio of DDC$^-$ + 0.5 mol Cu^{2+} should be noted. For simplicity, DDC$^-$/Cu^{2+} liposomes were entitled as Cu(DDC)$_2$ liposomes. This is justified by the fact, that Cu(DDC)$_2$ is formed by DDC$^-$ and Cu^{2+} in the aqueous core of liposomes and that Cu(DDC)$_2$ is responsible for the anticancer ctivity.

2.5. Liposome Characterization and Stability Measurement

2.5.1. Size and Polydispersity Index

The size expressed as the hydrodynamic diameter (d$_h$) and the polydispersity index (PDI) were measured via dynamic light scattering (DLS, ZetaPals, Brookhaven Instruments Corporation, Holtsville, NY, USA). Liposomal samples were diluted to 1–5 mM (total lipid) in filtered SH buffer for size and polydispersity analyses.

2.5.2. Cu(DDC)$_2$ to Lipid Ratio

The Cu(DDC)$_2$ to lipid ratio (drug to lipid ratio, *D/L*) was calculated with Equation (2), where $n_{entrapped\ drug}$ is the amount of substance of complexed DDC$^-$ with Cu^{2+} and $n_{total\ lipid}$ the amount of substance of lipid:

$$D/L\,[\mathrm{mol:mol}] = n_{entrapped\ drug}/n_{total\ lipid} \tag{2}$$

2.5.3. Liposomal Stability Studies

For storage stability studies the liposomes were kept at 4–6 °C for 6 months (183 days) and at RT (22 ± 2 °C) and −20 °C for 2 months (61 days). Therefore, aliquots of non-PEGylated and PEGylated Cu(DDC)$_2$ liposomes were prepared and characterized via DLS at the indicated time points. Stability studies included the determination of the release rate of Cu(DDC)$_2$ from liposomes after storage of samples at 4–6 °C for 6 months using surface area filtration (Section 2.3).

2.6. Cell Culture

LS, Kelly, and SH-SY5Y neuroblastoma cells, as well as primary human skeletal muscle cells (hSkMC) and primary human dermal fibroblasts, and adult (hDFa) were obtained as a kind gift from Professor Dr. Rupert Handgretinger (Universitätskinderklinik Tübingen, Germany). Cells were cultivated at 37 °C, 5% CO$_2$ in a humidified incubator in RPMI

supplemented with 10% FCS (LS, Kelly, SH-SY5Y, and hDFa) or DMEM supplemented with 5% sodium pyruvate and 10% FCS (hSkMC).

Next, 3D cell cultures were generated by the liquid overlay method [25]. Briefly, each well of a 96-well microtiter plate was coated under aseptic conditions with 50 µL of an autoclaved and therefore liquefied 1.5% (*w/v*) agarose–PBS solution. After cool down (to RT) and solidification of the agarose, 200 µL of a 20,000 cell/mL suspension was added per well. Following a centrifugation step at $600 \times g$, for 5 min at 20 °C, the plate was incubated for 72 h in an incubator (37 °C and 5% CO_2, humidified) until reaching a spheroid diameter of approximately 400 µm to start the liposomal treatment. Spheroid formation and growth were documented with an Axiovert 40 CFL microscope, an Axiocam 305 color camera, and a ZEN core v3.0 software via extended depth of focus (Carl Zeiss, Oberkochen, Germany). For co-culture spheroids, the cell number of a primary and a cancer cell dispersion was adjusted to a mixed cellular dispersion at a 1:1 ratio. LS-hDFa co-culture spheroids were cultivated in RPMI supplemented with 10% FCS and LS-hSkMC co-culture spheroids were cultivated in DMEM supplemented with 5% sodium pyruvate and 10% FCS.

2.7. Cell Viability Experiments

For 2D monolayer experiments neuroblastoma cells and primary cells were seeded in white opaque 96-well microtiter plates (Greiner Bio, Frickenhausen, Germany) in a density of 2000–7000 cells per well and cultured overnight. Cells were treated with $Cu(DDC)_2$ liposomes, free $Cu(DDC)_2$ and Cu^{2+}. After 24, 48, or 72 h of treatment, CellTiter-Glo® for 2D cell cultures was added according to the manufacturer's protocol. For 3D spheroid experiments, 3D cell cultures were generated as described in Section 2.6. Following 3 days of incubation in an incubator, spheroids were treated with $Cu(DDC)_2$ liposomes. After 72 h, the viability was determined with the CellTiter-Glo® assay for 3D cell cultures. EC_{50} (half maximal effective concentration) values were calculated by Excel solver and non-linear least squares fitting [26] with the following equation.

$$y = y_0 + \frac{y_{100} - y_0}{1 + \left(\frac{EC_{50}}{x}\right)^{-p}} \tag{3}$$

The cell viability (y) is calculated as concentration (x) in µM. The term y_{100} represents the viability of control cells, y_0 the lowest viability, and p the hill coefficient [27]. Cytotoxicity analyses were evaluated with at least three different data sets. The EC_{50} value is calculated as the mean of the generated EC_{50} values.

2.8. Epifluorescent Staining of 3D Spheroids

LS spheroids were cultured in RPMI 1640 medium w/o phenol red and treated with non-PEGylated or PEGylated $Cu(DDC)_2$ liposomes. Spheroids were stained with 1 µM calcein-AM and 5 µM PI for the last 2 h of a 72 h incubation period of $Cu(DDC)_2$ liposomes. Living and dead cells were analyzed with an Axiocam 305 color camera, a ZEN core v3.0 software (Carl Zeiss, Oberkochen, Germany), a 10× objective and a corresponding filter set for calcein-AM and propidium iodide.

2.9. Cellular Uptake Studies

Cellular association and uptake of non-PEGylated and PEGylated DiO liposomes were assessed via flow cytometry (BD LSRFortessa™, Becton Dickinson, Kelberg, Germany). DSPC:Chol:DiO [55:45 + 0.5 molar ratio] and DSPC:Chol:DSPE-mPEG$_{2000}$:DiO [50:45:5 + 0.5 molar ratio] liposomes, carrying DiO as the fluorescent label, were diluted with culture medium to reach a final lipid concentration of 0.75 mM. LS cells were seeded in 24 well plates at a density of 60,000 cells/mL and cultured overnight. Cells were incubated for 15 min, 1, 2, 4, and 6 h with DiO-labelled liposomes. After the incubation periods, cells were washed with ice cold PBS w/o Ca^{2+} and Mg^{2+}, trypsinized and detached from wells via resuspension in PBS buffer and collected in FACS tubes. The cells were analyzed using

a 488-nm blue laser for excitation and a 530/30-nm filter set. There were 10,000 events per sample recorded and cells were gated using forward and sideward scattering to determine the live cell population. Afterwards, the extracellular DiO fluorescence was quenched by the addition of 0.08% trypan blue [28] and the samples were repeatedly analyzed to distinguish cellular association and cellular uptake of DiO-labelled liposomes. The fluorescence intensity and the percentage of fluorescent cells (living gate) were evaluated.

2.10. Statistical Analysis

All data are expressed as mean $\pm$ SD. GraphPad Prism 8.01 software was used for statistical analysis. One-way ANOVA with Tukey's multiple comparison test was used to evaluate differences between unpaired data sets. One-way ANOVA with Dunnett's multiple comparison test was used to evaluate differences between the mean of each sample with the mean of the control (unpaired). Differences were considered significant when $p < 0.05$ (* < 0.05, ** < 0.01, *** < 0.001) in all analyses.

3. Results

3.1. Stability of Cu(DDC)$_2$ Liposomes

3.1.1. Validation of Non-Encapsulated Cu(DDC)$_2$ Precipitate Removal via Surface Area Filtration

The preparation process of Cu(DDC)$_2$ liposomes and the experimental set up for stability analyses was validated. Initially, liposomal agglomeration occurring after the preparation process of Cu(DDC)$_2$ liposomes was noticed via DLS and Cryo-TEM (data not shown). This was mainly due to the presence of extraliposomal (non-encapsulated) precipitated Cu(DDC)$_2$ which agglomerates with liposomes due to the lipophilicity of the Cu(DDC)$_2$ complex. Therefore, surface area filtration was introduced as the final step in the preparation process to retain extraliposomal Cu(DDC)$_2$ from Cu(DDC)$_2$ liposomes. This approach had to be validated to ensure extraliposomal Cu(DDC)$_2$ retention without lipid loss. Figure 2a shows a schematic representation of the validation process with 1st + 2nd filtration as part of the liposomal preparation process and a 3rd and 4th filtration to test consecutive filtration without affecting the D/L ratio and reducing the lipid amount of the liposomal dispersion. The results were evaluated statistically via one-way ANOVA and Tukey's multiple comparison test. The validation analysis was performed with non-PEGylated (DSPC:Chol [55:45 molar ratio]) and PEGylated (DSPC:Chol:DSPE-mPEG$_{2000}$ [50:45:5 molar ratio]) Cu(DDC)$_2$ liposomes (Figure 2b). A reduction of the D/L ratio was noted before and after 1st + 2nd filtration for non-PEGylated and PEGylated Cu(DDC)$_2$ liposomes, whereas the lipid amount remained constant. No significant differences in D/L ratios and lipid amounts were detected for both formulations between the 1st + 2nd filtration and 3rd filtration. Non-PEGylated liposomes revealed a slight significant difference among the D/L ratios ($p = 0.0104$) between the 1st + 2nd filtration and 4th filtration. Overall, the lipid amount did not change for neither non-PEGylated nor PEGylated Cu(DDC)$_2$ liposomes during consecutive filtration through 0.2-μm CA filters and no significant change of the D/L ratio was observed after the 3rd filtration step.

3.1.2. In Vitro Colloidal Stability and Drug Release Analysis of Cu(DDC)$_2$ Liposomes

As described in Section 2.2, non-PEGylated and PEGylated Cu(DDC)$_2$ liposomes were prepared via the thin film hydration method with subsequent extrusion. Non-PEGylated Cu(DDC)$_2$ liposomes showed a d_h of 156 ± 7 nm, a PDI of 0.16 ± 0.02, and a D/L ratio of 0.15 ± 0.03 mol:mol. PEGylated Cu(DDC)$_2$ liposomes exhibited a d_h of 161 ± 7 nm, a PDI of 0.14 ± 0.01, and a D/L ratio of 0.30 ± 0.04 mol:mol (Table 1).
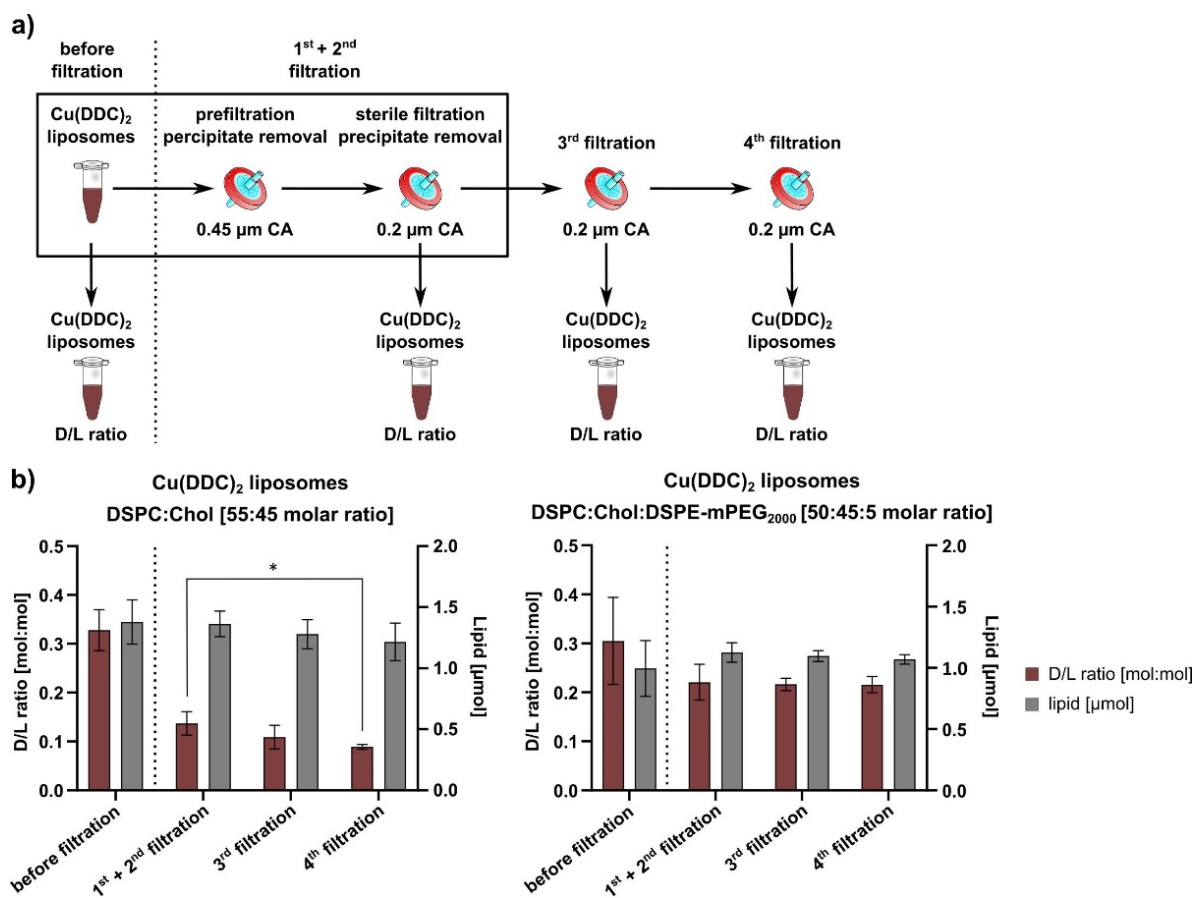
Figure 2. Validation analysis of the removal of extraliposomal $Cu(DDC)_2$ via surface area filtration. (**a**) Experimental procedure of testing consecutive filtration steps for the removal of extraliposomal $Cu(DDC)_2$. The 1st + 2nd filtration was part of the liposome preparation process. The 3rd and 4th filtration were conducted to determine the limit of filtration steps until affecting liposomal stability. Aliquots were collected after each step to determine the D/L ratio and lipid amount. (**b**) The D/L ratio and lipid amount of non-PEGylated and PEGylated liposomes were analyzed after consecutive filtration steps and evaluated statistically via one-way ANOVA and Tukey's multiple comparison test (* $p = 0.0104$). Data are expressed as the mean $\pm$ SD ($n = 3$–4).

Table 1. Hydrodynamic diameter (d_h), polydispersity index (PDI), and D/L ratio of prepared liposomes. Data are expressed as the mean $\pm$ SD ($n = 7$).

Liposomes	d_h [nm]	PDI	D/L Ratio [mol:mol]
Non-PEGylated Cu^{2+} liposomes (DSPC:Chol)	119 ± 3	0.06 ± 0.02	-
PEGylated Cu^{2+} liposomes (DSPC:Chol:DSPE-mPEG$_{2000}$)	116 ± 5	0.08 ± 0.02	-
Non-PEGylated $Cu(DDC)_2$ liposomes (DSPC:Chol)	156 ± 7	0.16 ± 0.02	0.15 ± 0.03
PEGylated $Cu(DDC)_2$ liposomes (DSPC:Chol:DSPE-mPEG$_{2000}$)	161 ± 7	0.14 ± 0.01	0.30 ± 0.04

Particle size, size distribution, and drug retention are critical parameters during storage. Therefore, aliquots of $Cu(DDC)_2$ liposomes were stored (in SH buffer) for 6 months (183 days) at 4–6 °C (Figure 3a) and for 2 months (61 days) at RT (22 ± 2 °C; Figure 3b) and −20 °C (Figure 3c) and analyzed for size and size distribution. Data was evaluated statistically using one-way ANOVA and Dunnett's post-hoc test by comparing the mean

of each d_h-column with the mean of the control d_h-column (t = 0 days). For Cu(DDC)$_2$ liposomes, stored at 4–6 °C, a significant difference in d_h was observed after 3 months (91 days) for non-PEGylated ($p < 0.001$) and after 6 months for PEGylated Cu(DDC)$_2$ liposomes ($p = 0.006$) compared to freshly prepared preparations. Figure 3b shows initial instabilities after 14 days for non-PEGylated ($p = 0.02$) and after 28 days for PEGylated Cu(DDC)$_2$ liposomes ($p = 0.01$) stored at RT. After one day storage at −20 °C non-PEGylated ($p < 0.001$) and PEGylated ($p < 0.001$) Cu(DDC)$_2$ liposomes exhibited increasing instability. The storage temperature of 4–6 °C resulted in constant size and size distribution for non-PEGylated and PEGylated Cu(DDC)$_2$ liposomes.

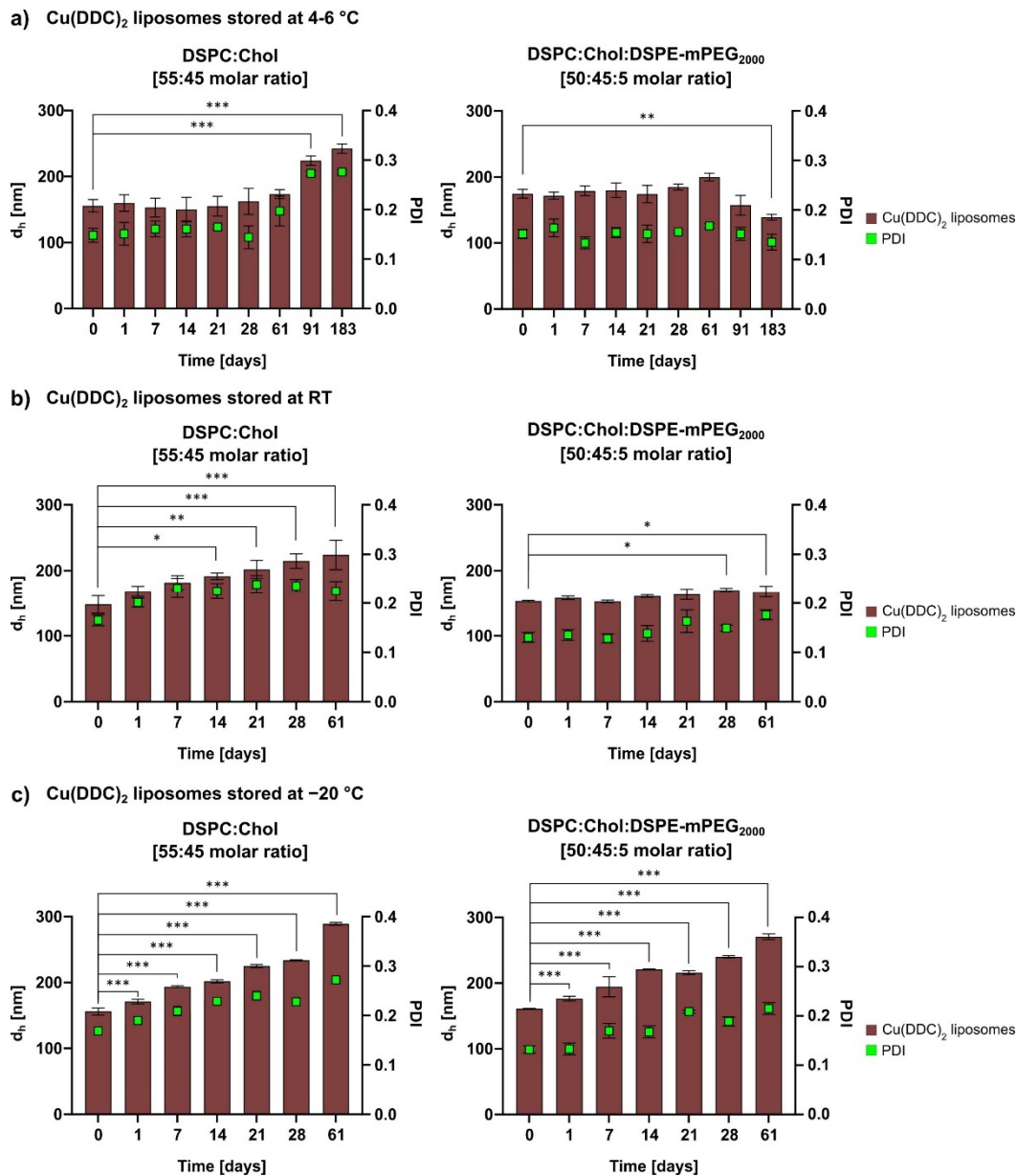**Figure 3.** Colloidal stability analysis of Cu(DDC)$_2$ liposomes after different storage conditions. Aliquots of non-PEGylated and PEGylated Cu(DDC)$_2$ liposomes were analyzed via dynamic light scattering (DLS) over 6 months (183 days) at 4–6 °C (**a**) and over 2 months (61 days) at RT (**b**) and −20 °C (**c**). Significant differences were evaluated via one-way ANOVA and Dunnett's post-hoc test (* $p \leq 0.05$; ** $p \leq 0.01$; *** $p \leq 0.001$). Data are expressed as the mean ± SD ($n = 3$).

After the determination of a suitable storage temperature, it had to be proven that Cu(DDC)$_2$ does not leak out of liposomes in the timeframe between preparation, storage,

and actual administration. Therefore, aliquots of non-PEGylated and PEGylated Cu(DDC)$_2$ liposomes were adjusted to equal D/L ratios and stored for 6 months at 4–6 °C. The liposomal aliquots were refiltrated through a 0.2-µm CA filter after specific storage periods and the D/L ratio of the filtrates was determined. A decrease in D/L ratio indicated Cu(DDC)$_2$ release. The mean D/L ratio of t = 0 days was defined as control (100%), so the collected data is expressed as % of control and plotted against the time (t = 0–183 days; Figure 4). PEGylated Cu(DDC)$_2$ liposomes displayed 90–100% drug retention until 3 months of storage, which decreased to 74% after 6 months of storage. For non-PEGylated Cu(DDC)$_2$ liposomes the drug retention decreased to 54% after 7 days and furthermore to 15% after 6 months.

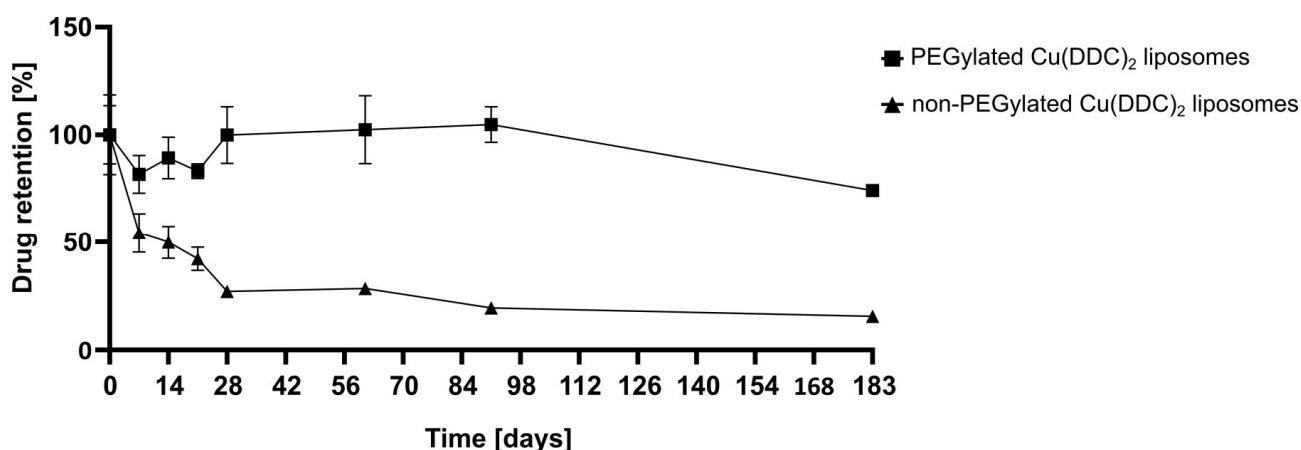**Figure 4.** Liposomal Cu(DDC)$_2$ retention upon storage at 4–6 °C. Aliquots of non-PEGylated and PEGylated Cu(DDC)$_2$ liposomes (8 mM total lipid) were stored at 4–6 °C for 6 months (183 days). Samples were filtered through a 0.2-µm CA filter after specific storage time points. The D/L ratio of Cu(DDC)$_2$ liposomes was determined before and after the filtration step. A reduction of the D/L ratio indicated Cu(DDC)$_2$ release from liposomes. Data are expressed as the mean ± SD (*n* = 3).

3.2. In Vitro Determination of the Cytotoxicity of Cu(DDC)$_2$ Liposomes, Free Cu^{2+} and Cu(DDC)$_2$, and the Evaluation of Liposomal Uptake in Neuroblastoma 2D Monolayers

The cytotoxic potency of Cu(DDC)$_2$ liposomes was compared to free Cu(DDC)$_2$ and free Cu^{2+}. Therefore, cell viability was determined in Kelly and SH-SY5Y (neuroblastoma cells) using the 2D CellTiter-Glo® assay (Figure 5a,b). EC$_{50}$ values of liposomal Cu(DDC)$_2$, free Cu(DDC)$_2$, and Cu^{2+} achieved with Kelly cells were in a concentration range of 0.12 ± 0.01 µM, 0.42 ± 0.03 µM, and 427.19 ± 8.86 µM and for SH-SY5Y in a concentration range of 0.13 ± 0.02 µM, 0.37 ± 0.09 µM, and 483.80 ± 62.07 µM, respectively. Notably, the cytotoxic effect of liposomal Cu(DDC)$_2$ was higher than free Cu(DDC)$_2$ on neuroblastoma cell lines (EC$_{50}$ of Cu(DDC)$_2$ liposomes: 0.12 ± 0.01 µM (Kelly), 0.13 ± 0.02 µM (SH-SY5Y); EC$_{50}$ of free Cu(DDC)$_2$: 0.42 ± 0.03 µM (Kelly), and 0.37 ± 0.09 µM (SH-SY5Y)). Cu^{2+} revealed cytotoxic effects in a concentration range significantly exceeding the applied Cu^{2+} concentration in liposomal Cu(DDC)$_2$ formulations (Figure 5c,d).

Furthermore, in vitro cellular uptake experiments were conducted on LS monolayers with 0.75 mM non-PEGylated and PEGylated DiO liposomes and determined via flow cytometry (Figure 6). Cells were treated for 15 min, 1, 2, 4, and 6 h with DiO liposomes. The cellular uptake was rather low in the first hours and reached 24.8 ± 5.2% for non-PEGylated DiO liposomes and 17.8 ± 3.0% for PEGylated DiO liposomes after 6 h of incubation. A similar cellular fluorescence intensity was measured for both formulations.
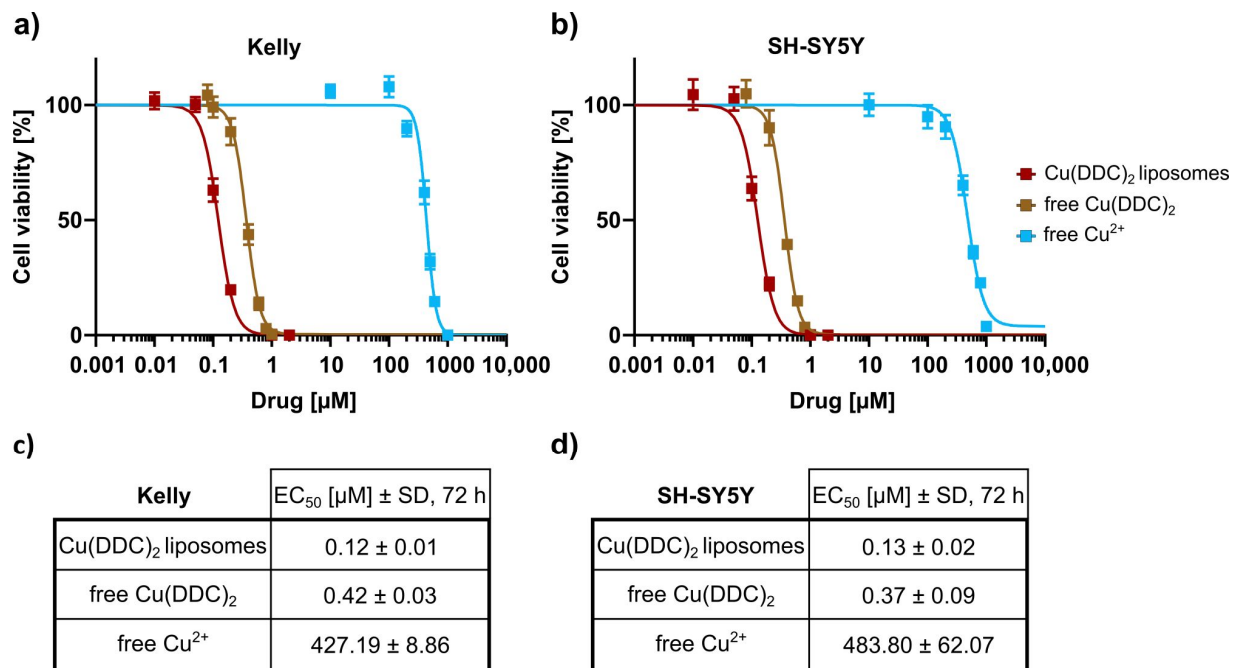
Figure 5. Determination of the cell viability reduction of Cu(DDC)$_2$ liposomes and the free substances Cu(DDC)$_2$ and Cu^{2+} on 2D monoculture neuroblastoma cell models. (**a**,**b**) 2D Kelly (**a**) and SH-SY5Y (**b**) monolayers were treated with liposomal Cu(DDC)$_2$ (DSPC:Chol [55:45 molar ratio]), free Cu(DDC)$_2$ and free Cu^{2+}. Cell viability curves were obtained using 2D CellTiter-Glo® assay after 72 h of treatment. Data are expressed as the mean ± SD (*n* = 3–4). (**c**,**d**) EC$_{50}$ values after 72 h of treatment with liposomal Cu(DDC)$_2$, free Cu(DDC)$_2$, and free Cu^{2+}. Data are expressed as the mean ± SD (*n* = 3–4).

▲ DSPC:Chol:DiO [55:45 + 0.5 molar ratio]

■ DSPC:Chol:DSPE-mPEG$_{2000}$:DiO [50:45:5 + 0.5 molar ratio]
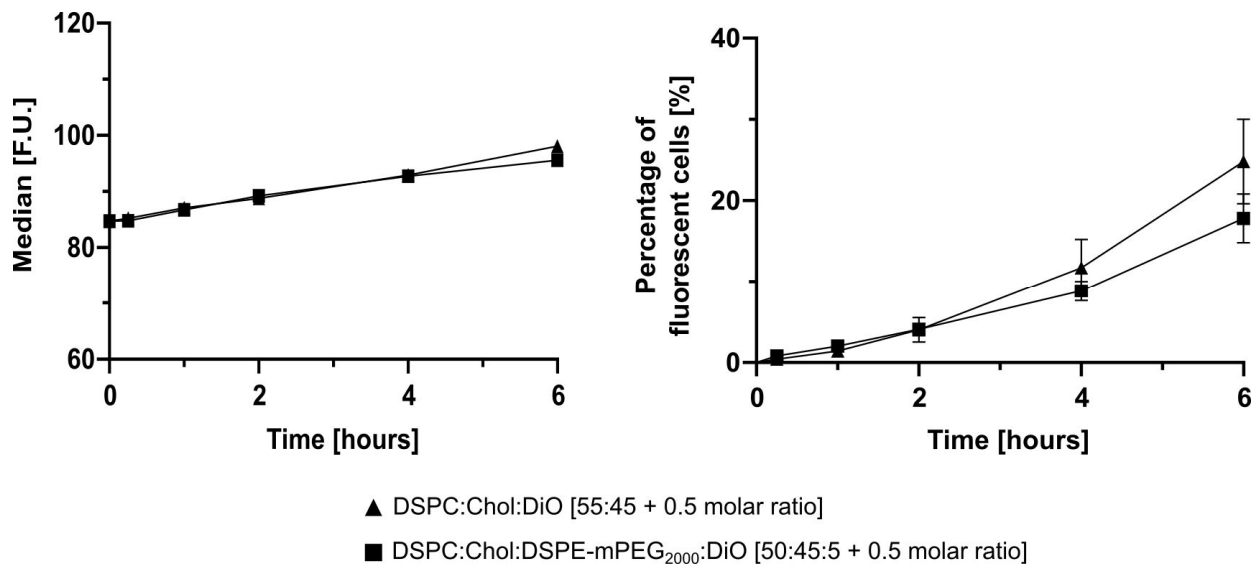
Figure 6. Cellular uptake of DiO labelled liposomes by 2D LS monocultures. 2D LS monolayers were incubated with non-PEGylated and PEGylated DiO labelled liposomes for 15 min, 1, 2, 4, and 6 h. Cellular uptake was evaluated via flow cytometry. The percentage of fluorescent cells (living gate) showed 24.8 ± 5.2% uptake for non-PEGylated and 17.8 ± 3.0% for PEGylated DiO liposomes. Data are expressed as the mean ± SD (*n* = 3).

3.3. Cytotoxicity and Selectivity of Cu(DDC)$_2$ Liposomes on 2D and 3D Cell Cultures

Drug potency and selectivity of Cu(DDC)$_2$ liposomes were evaluated with LS neuroblastoma and primary hSkMC and hDFa cells using 2D monolayers and 3D spheroids. Initially, the cytotoxic potency was analyzed in 2D LS monolayers after 24, 48, and 72 h of incubation with non-PEGylated and PEGylated Cu(DDC)$_2$ liposomes (Figure 7). The

cell viability was quantified via the 2D CellTiter-Glo® assay. Statistical analyzes were performed with one-way ANOVA and Tukey's multiple comparison test. The resulting EC_{50} values for 24, 48, and 72 h were in a concentration range of 0.16 ± 0.01 μM, 0.06 ± 0.01 μM, and 0.05 ± 0.02 μM for non-PEGylated and 0.13 ± 0.01 μM, 0.04 μM, and 0.07 ± 0.02 μM for PEGylated $Cu(DDC)_2$ liposomes, respectively. $Cu(DDC)_2$ liposomes affected the cell viability in a concentration and time dependent manner (Figure 7a,b), whereby the calculated EC_{50} values after 48 and 72 h of treatment did not vary significantly (48 vs. 72 h EC_{50} of non-PEGlyated liposomes: $p = 0.71$; 48 vs. 72 h EC_{50} of PEGylated liposomes: $p = 0.21$; Figure 7c,d). No difference in cytotoxic potency was observed comparing non-PEGylated and PEGylated $Cu(DDC)_2$ liposomes.
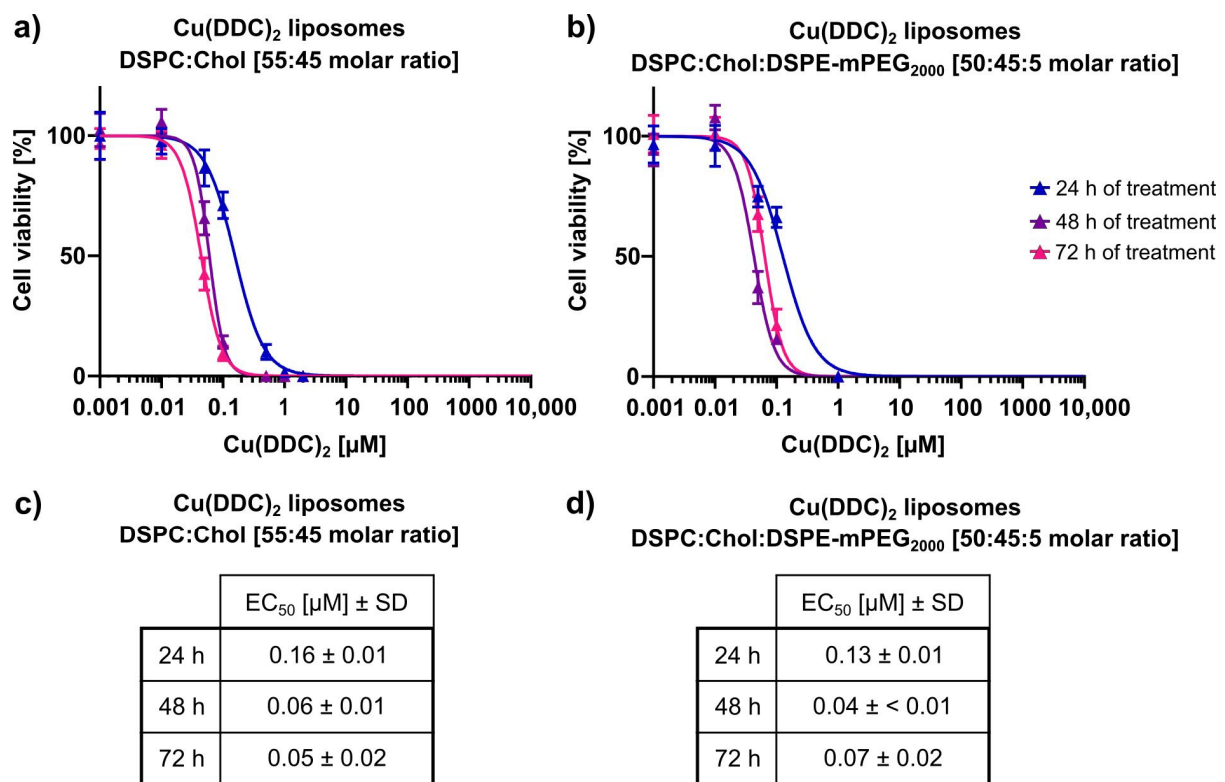

Figure 7. In vitro cytotoxicity of liposomal $Cu(DDC)_2$ on 2D LS monoculture cells. (**a**,**b**) LS monolayers were incubated with non-PEGylated (**a**) and PEGylated (**b**) $Cu(DDC)_2$ liposomes for 24, 48, and 72 h. Cell viability was analyzed using the 2D CellTiter-Glo® assay after indicated treatment duration. (**c**,**d**) EC_{50} values after 24, 48, and 72 h of treatment with non-PEGylated (**c**) and PEGylated (**d**) $Cu(DDC)_2$ liposomes. Data are expressed as the mean $\pm$ SD ($n = 3$–7).

Furthermore, cell viability of 3D LS spheroids was analyzed 72 h after treatment with $Cu(DDC)_2$ liposomes via the 3D CellTiter-Glo® assay. 3D spheroids were generated as described in Section 2.6 via the liquid overlay technique resulting in dense spheroids with a highly reproducible diameter and an inter plate coefficient of variation less than 3% [27]. $Cu(DDC)_2$ liposomes affected the cell viability of 3D LS spheroids dose-dependently (Figure 8a,b). Non-PEGylated $Cu(DDC)_2$ liposomes revealed an EC_{50} value of 4.09 ± 0.01 μM and PEGylated $Cu(DDC)_2$ liposomes of 3.95 ± 0.80 μM when used on 3D LS spheroids. Hence, the resulting EC_{50} values were far higher in comparison to those of 2D LS monolayers (Figure 8c,d). Microscopy images of 3D LS spheroids were taken over time during treatment with $Cu(DDC)_2$ liposomes (Figure 8e,f). Surprisingly, treatment with non-PEGylated liposomes led to complete disintegration of the spheroids, whereby treatment with PEGylated liposomes resulted in maintenance of the spherical shape.
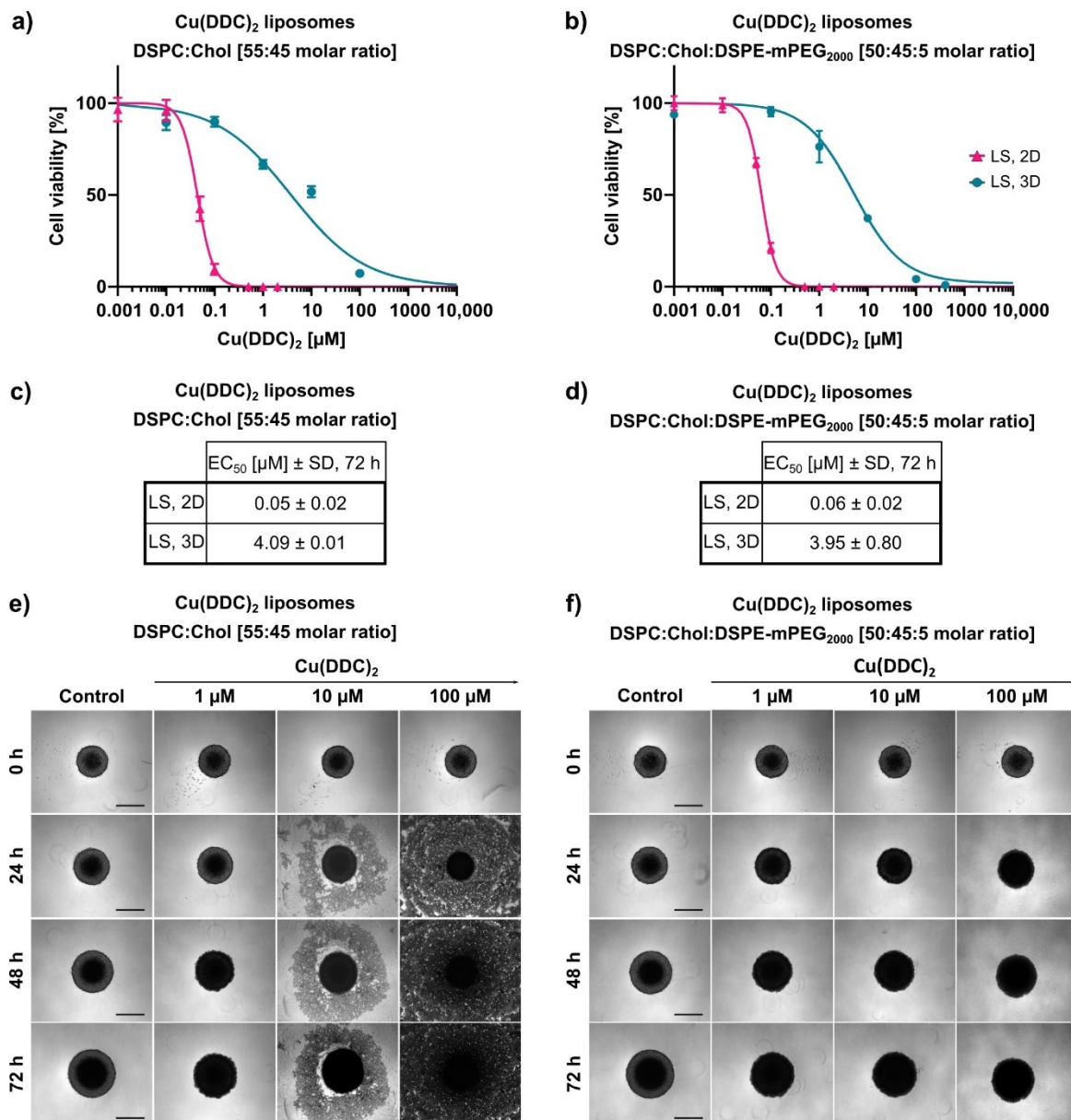
Figure 8. In vitro cytotoxicity of $Cu(DDC)_2$ liposomes on neuroblastoma 2D and 3D cell cultures. (**a**,**b**) LS monolayers (2D) and LS monoculture spheroids (3D) were treated 72 h with non-PEGylated (**a**) and PEGylated (**b**) $Cu(DDC)_2$ liposomes. 3D spheroids were generated by using agarose-coated wells with subsequent centrifugation. Cell viability curves were obtained using 2D and 3D CellTiter-Glo® assay, respectively after indicated treatment duration. Data are expressed as the mean ± SD (LS, 2D: *n* = 7; LS, 3D: *n* = 5). (**c**,**d**) EC_{50} values after 72 h of treatment with non-PEGylated (**c**) and PEGylated (**d**) $Cu(DDC)_2$ liposomes. Data are expressed as the mean ± SD (*n* = 5–7). (**e**,**f**) Representative brightfield microscopy images of LS monoculture spheroids. Images were taken after 24, 48, and 72 h of treatment with non-PEGylated (**e**) and PEGylated (**f**) $Cu(DDC)_2$ liposomes, respectively. Scale bar = 400 μm.

Live/dead staining of 3D LS spheroids allowed to distinguish between proliferating and dead cells to further evaluate the influence of $Cu(DDC)_2$ liposomes (Figure 9). Therefore, 3D LS spheroids were stained with calcein-AM and PI for the last 2 h of a 72 h incubation period with $Cu(DDC)_2$ liposomes and compared with untreated spheroids being incubated with cell medium for the same duration of time (72 h total). The untreated control revealed a typical architecture of a dense spheroid containing a necrotic core (red) surrounded by an outer rim consisting of proliferating cells (green; Figure 9). This cellular arrangement changed dose dependently after treatment with $Cu(DDC)_2$ liposomes, result-

ing in an increasing portion of dead cells, according to the viability analyses (Figure 8). Single detached dead cells were visible after administration of low liposomal $Cu(DDC)_2$ dosages. With increasing concentration of $Cu(DDC)_2$ liposomes the PI signal intensified in the outer proliferating cell layer until it reached the necrotic core (Figure 9).
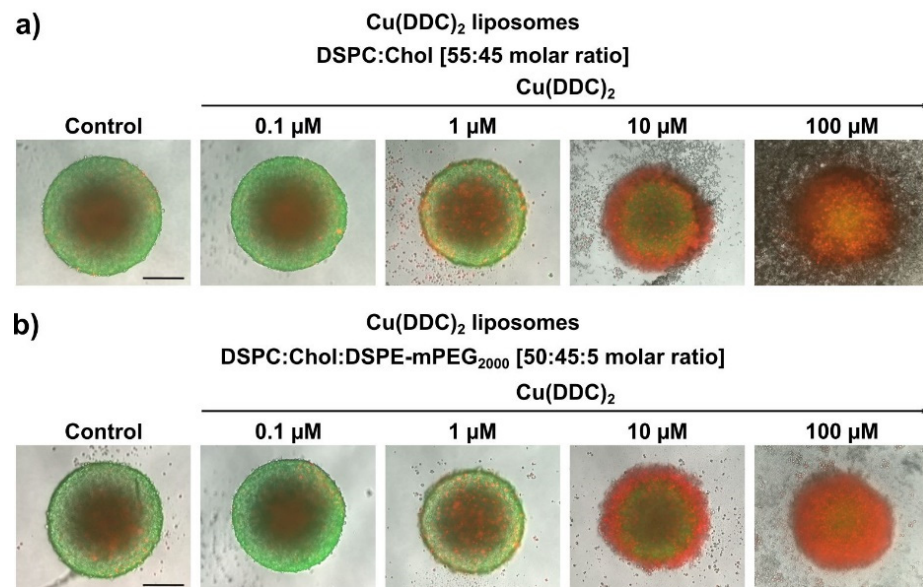

Figure 9. Representative fluorescence microscopy images of 3D LS monoculture spheroids on the basis of live/dead staining. 3D LS spheroids were treated for 72 h with non-PEGylated (**a**) and PEGylated (**b**) $Cu(DDC)_2$ liposomes. The spheroids were stained with a combination of two dyes: 1 μM calcein-AM and 5 μM PI, added 2 h prior to the end of liposomal treatment. Calcein-AM (green) is visible at the outer cell layer, indicating highly proliferating and viable cells. PI (red) is primarily located in the inner core, indicating necrotic and dead cells. With increasing doses of $Cu(DDC)_2$ liposomes, the PI signal intensified in the outer proliferating cell layer, until reaching the necrotic core. Scale bar = 200 μm.

In a next step, the cytotoxicities of non-PEGylated and PEGylated $Cu(DDC)_2$ liposomes were examined by using non-malignant cells. 2D monolayers of hSkMC as well as hDFa were incubated for 24 h with $Cu(DDC)_2$ liposomes. The cell viability was analyzed via the 2D CellTiter-Glo® assay (Figure 10a,b) and compared to the cell viability of treated LS monolayers. Calculated EC_{50} values (Figure 10c,d) were analyzed statistically via one-way ANOVA and Tukey's multiple comparison test. hSkMC and hDFa displayed significantly higher EC_{50} values in comparison to LS cells after treatment with $Cu(DDC)_2$ liposomes (hSkMC vs. LS with non-PEGylated liposomes: $p < 0.001$ and PEGylated liposomes: $p = 0.004$; hDFa vs. LS with non-PEGylated liposomes: $p < 0.001$ and PEGylated liposomes: $p < 0.001$). The hDFa cells displayed higher EC_{50} values compared to hSkMC cells (EC_{50} of non-PEGylated $Cu(DDC)_2$ liposomes: 0.28 ± 0.01 μM (hSkMC) and 0.51 ± 0.03 μM (hDFa); EC_{50} of PEGylated $Cu(DDC)_2$ liposomes: 0.38 ± 0.07 μM (hSkMC) and 0.61 ± 0.02 μM (hDFa); Figure 10c,d). Moreover, hSkMC and hDFa were more sensitive to non-PEGylated compared to PEGylated $Cu(DDC)_2$ liposomes. Anyhow, the viability of non-malignant cells was affected by $Cu(DDC)_2$ liposomes in a dose dependent manner.

a) Cu(DDC)$_2$ liposomes DSPC:Chol [55:45 molar ratio]

b) Cu(DDC)$_2$ liposomes DSPC:Chol:DSPE-mPEG$_{2000}$ [50:45:5 molar ratio]

c) Cu(DDC)$_2$ liposomes DSPC:Chol [55:45 molar ratio]

	EC$_{50}$ [µM] ± SD, 24 h
LS	0.16 ± 0.01
hSkMC	0.28 ± 0.01
hDFa	0.51 ± 0.03

d) Cu(DDC)$_2$ liposomes DSPC:Chol:DSPE-mPEG$_{2000}$ [50:45:5 molar ratio]

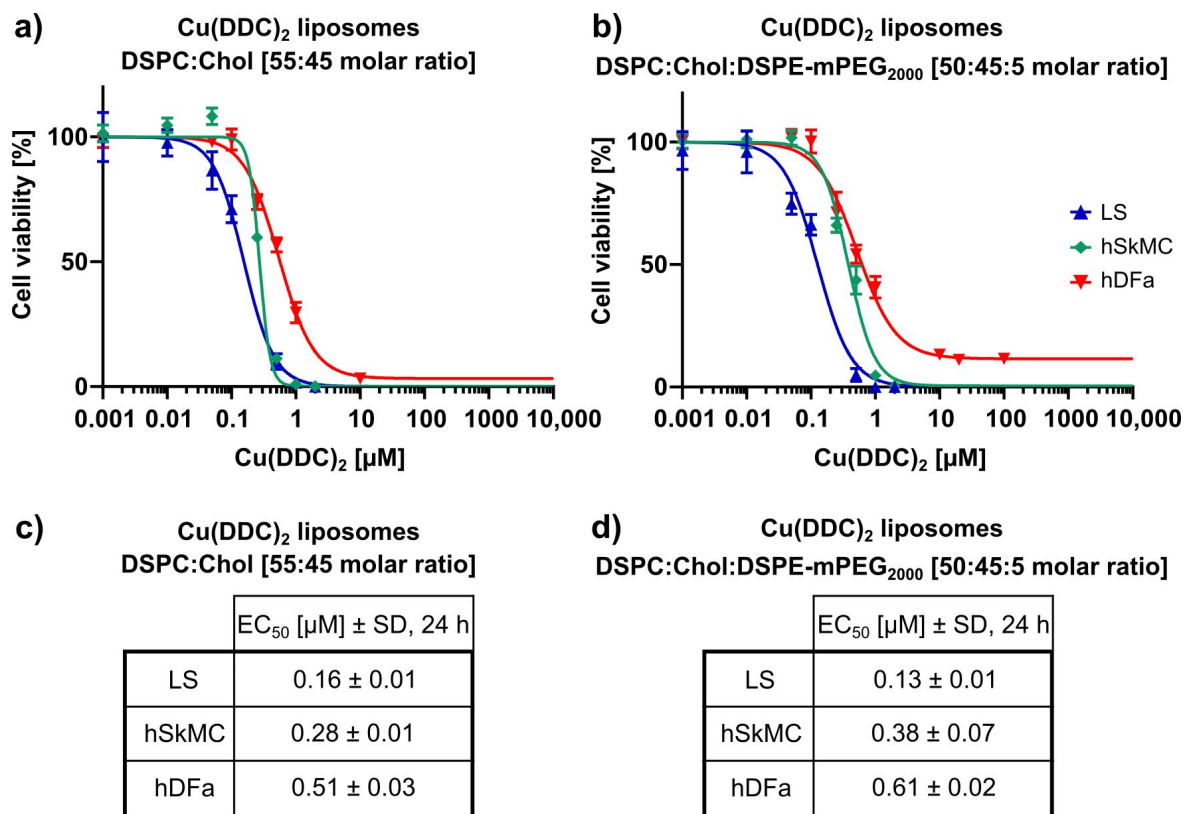|	EC$_{50}$ [µM] ± SD, 24 h
LS	0.13 ± 0.01
hSkMC	0.38 ± 0.07
hDFa	0.61 ± 0.02

Figure 10. In vitro cytotoxicity of Cu(DDC)$_2$ liposomes on 2D hSkMC and 2D hDFa monoculture cell models. (**a,b**) 2D monolayers of LS, hSkMC, and hDFa cells were incubated with non-PEGylated (**a**) and PEGylated (**b**) Cu(DDC)$_2$ liposomes for 24 h. Cell viability was analyzed using the 2D CellTiter-Glo® assay after indicated treatment duration. (**c,d**) EC$_{50}$ values after 24 h of treatment with non-PEGylated (**c**) and PEGylated (**d**) Cu(DDC)$_2$ liposomes. Data are expressed as the mean ± SD (*n* = 3).

3D LS spheroids were also generated as co-culture with hSkMC as well as hDFa to analyze the cytotoxic effectiveness of Cu(DDC)$_2$ liposomes. Consequently, 3D co-culture spheroids were also treated for 72 h with non-PEGylated and PEGylated Cu(DDC)$_2$ liposomes. The viability was determined via the 3D CellTiter Glo® assay, resulting in similar cytotoxic responses as determined in the tested cell lines (Figure 11a,b). Statistical analysis between EC$_{50}$ values via one-way ANOVA and Tukey's multiple comparison test confirmed the absence of significance (EC$_{50}$ values from LS vs. LS-hSkMC vs. LS-hDFa: *p* = 0.46 (non-PEGylated Cu(DDC)$_2$ liposomes), *p* = 0.48 (PEGylated Cu(DDC)$_2$ liposomes); Figure 11c,d). Figure 11e,f depicts brightfield images of mono- and co-culture spheroids after 72 h of treatment with Cu(DDC)$_2$ liposomes. According to Figure 8e,f, the same morphological changes of 3D spheroids can be observed after treatment with Cu(DDC)$_2$ liposomes. Treatment with non-PEGylated Cu(DDC)$_2$ liposomes led to spheroid disintegration, whereby treatment with PEGylated Cu(DDC)$_2$ liposomes resulted in the maintenance of the spherical shape.
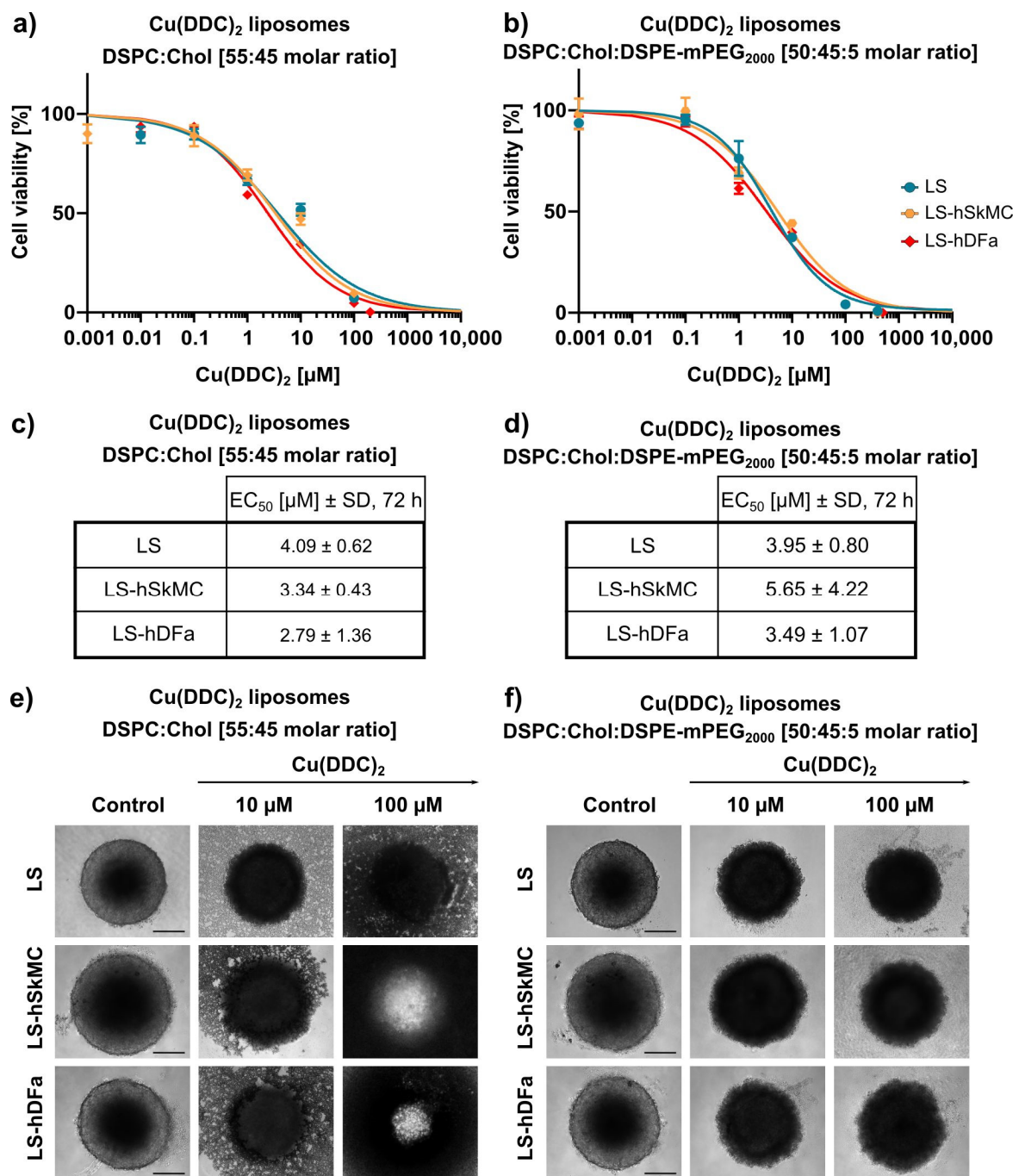
Figure 11. In vitro cytotoxicity of $Cu(DDC)_2$ liposomes on LS-hSkMC and LS-hDFa co-culture spheroids. (**a**,**b**) LS monoculture spheroids, LS-hSkMC and LS-hDFa co-culture spheroids were treated 72 h with non-PEGylated (**a**) and PEGylated (**b**) $Cu(DDC)_2$ liposomes. 3D spheroids were generated by using agarose-coated wells with subsequent centrifugation. hSkMC and hDFa cells are mixed with LS cells in a 1:1 ratio for co-culture spheroids, respectively. Cell viability curves were obtained using the 3D CellTiter-Glo® assay after indicated treatment duration. (**c**,**d**) EC_{50} values after 72 h of treatment with non-PEGylated (**c**) and PEGylated (**d**) $Cu(DDC)_2$ liposomes. Data are expressed as the mean $\pm$ SD ($n = 3$). (**e**,**f**) Representative brightfield microscopy images of LS monoculture and co-culture spheroids with hSkMC and hDFa, respectively. Images were taken after 72 h of treatment with non-PEGylated (**e**) and PEGylated (**f**) $Cu(DDC)_2$ liposomes. Scale bar = 200 μm.

4. Discussion and Outlook

In this study, liposomes were used as a drug delivery system for the water-insoluble $Cu(DDC)_2$ complex which exhibits cytotoxic effects on cancer cells. A reproducible preparation process of $Cu(DDC)_2$ liposomes was developed on the basis of the publication of

Wehbe et al. (2016) [8]. The first part of this paper describes the additional integration of surface area filtration into the liposomal preparation process as a suitable method to remove extraliposomal $Cu(DDC)_2$ precipitates from $Cu(DDC)_2$ liposomes without lipid loss. It was proven that further consecutive filtration steps had no impact on the D/L ratio of $Cu(DDC)_2$ liposomes. Therefore, surface area filtration might also be considered as an in-process control step to evaluate and retain eventually released $Cu(DDC)_2$ from $Cu(DDC)_2$ liposomes after stress exposure (e.g., heat or storage), without affecting the D/L ratio by itself. Furthermore, the colloidal stability and drug release upon storage of non-PEGylated (DSPC:Chol [55:45 molar ratio]) and PEGylated (DSPC:Chol:DSPE-mPEG$_{2000}$ [50:45:5 molar ratio]) $Cu(DDC)_2$ liposomes were compared. In general, the physical stability of a liposomal dispersion is affected by changes in liposomal size due to aggregation and fusion and the leakage of entrapped drug. These physical instabilities originate from oxidation and hydrolysis of the liposomal constituents. Hence, the determination of the liposomal size and size distribution is a sensitive indicator of the physical liposomal stability [29]. The colloidal stability of $Cu(DDC)_2$ liposomes were evaluated at different storage temperatures (4–6 °C, RT, and −20 °C) in the presence of an SH buffer. An ideal storage temperature of 4–6 °C for liposomes was confirmed in various studies [30,31]. Furthermore, in this study, it was shown that a constant colloidal stability of non-PEGylated and PEGylated $Cu(DDC)_2$ liposomes were achieved at a storage temperature of 4–6 °C. Increasing instabilities were observed while storing at RT and −20 °C, despite the presence of a cryoprotective disaccharide (sucrose) in the liposomal buffer. In particular, storage at −20 °C could lead to mechanical stresses due to the formation of ice crystals during freezing. Buffers with glycerol and carbohydrates (e.g., trehalose) are reported to be more suitable for freezing liposomal dispersions in a temperature range between −20 and −30 °C [32]. However, it is recommended to store $Cu(DDC)_2$ liposomes at 4–6 °C, since this condition already reduces temperature-dependent hydrolysis and further cooling down of the preparation did not improve stability [29]. Moreover, the integration of hydrophilic PEG polymers on the surface of $Cu(DDC)_2$ liposomes not only resulted in higher D/L ratios, it also improved the colloidal stability during storage at 4–6 °C, probable through steric [33] and electrostatic repulsion [34]. Also, PEGylated $Cu(DDC)_2$ liposomes displayed a higher drug retention upon storage at 4–6 °C in comparison to non-PEGylated $Cu(DDC)_2$ liposomes. Thus, the usage of PEGylated $Cu(DDC)_2$ liposomes is recommended due to higher membrane stability. Overall, the presence of DSPE-mPEG$_{2000}$ can significantly modify characteristics of a liposomal formulation (e.g., increased entrapment efficiencies and higher drug retentions) [35]. In future studies, further impacts (e.g., pH, oxygen, and light) have to be examined to fully analyze the stability and degradation profile of $Cu(DDC)_2$ liposomes during storage. In addition, it is recommended to support stability analysis (conducted via DLS) with Cryo-TEM images. For long term storage of $Cu(DDC)_2$ liposomes, lyophilization can be taken into consideration. Furthermore, serum stability should be tested to further evaluate $Cu(DDC)_2$ liposomes for future in vivo experiments.

In the second part of this study, the in vitro cytotoxicity of $Cu(DDC)_2$ liposomes on 2D and 3D neuroblastoma cell models was examined. Initially it was shown, that liposomal $Cu(DDC)_2$ was more cytotoxic for 2D neuroblastoma cell cultures than free $Cu(DDC)_2$, which highlights the usage of a liposomal $Cu(DDC)_2$ formulation. Furthermore, the viability reduction of neuroblastoma cells could be attributed to the $Cu(DDC)_2$ complex, since the corresponding concentration of free Cu^{2+} did not affect the cell viability by itself. Beyond that, non-PEGylated and PEGylated $Cu(DDC)_2$ liposomes efficiently affected the viability of 2D LS monolayers in a time- and concentration-dependent manner. However, the resulting EC$_{50}$ values achieved for both formulations after 48 and 72 h of liposomal incubation did not differ significantly. Tawari et al. (2015) claimed, that $Cu(DDC)_2$ induces the cell death in a direct phase and in a delayed phase [36]. In the direct phase, cell viability is reduced via the formation of reactive oxygen species (ROS) which damages cells [18,34]. In the delayed phase, $Cu(DDC)_2$ interferes with essential molecular signaling pathways inducing apoptosis [36]. Consequently, the cellular ATP level rises, since the induction of

apoptosis requires energy [37]. Therefore, it is possible, that the cell viability (measured via an ATP-dependent assay) is not significantly reduced after 72 h of incubation compared to 48 h of incubation with Cu(DDC)$_2$ liposomes, due to the delayed phase of the cell death induction triggered by Cu(DDC)$_2$.

The cytotoxic effectiveness of Cu(DDC)$_2$ liposomes were further determined in more complex 3D LS monoculture spheroids. Surprisingly, treatment with non-PEGylated and PEGylated Cu(DDC)$_2$ liposomes lead to a distinct change in spheroid morphology. During treatment with non-PEGylated Cu(DDC)$_2$ liposomes a disintegration of the spheroid structure was observed where dead cells detached from the spheroid. No disintegration of the spheroid morphology was observed during the treatment of PEGylated Cu(DDC)$_2$ liposomes. However, the treatment with non-PEGylated Cu(DDC)$_2$ liposomes leads to the same extent of a complete viability reduction throughout different cell layers of the spheroid as with PEGylated Cu(DDC)$_2$ liposomes. This outcome implies high drug effectivity of the Cu(DDC)$_2$ formulations. Anyhow, a question arises about how the treatment with both Cu(DDC)$_2$ formulations can result in different spheroid morphologies. On the one hand, it is reported, that PEGylated liposomes could not interact with the spheroid due to PEG chains hindering an intratumoral transport [38]. This supports the suggestion that the different interactions of non-PEGylated and PEGylated Cu(DDC)$_2$ liposomes with cells or the spheroid could lead to distinct spheroid morphologies after treatment. On the other hand, Niora et al. (2020) described that PEGylated liposomes penetrate better into deeper cell layers of a spheroid due to poor interactions with cells compared to non-PEGylated liposomes [39]. Therefore, it is not clear whether non-PEGylated and PEGylated Cu(DDC)$_2$ liposomes accumulate at the spheroid surface or whether Cu(DDC)$_2$ liposomes are able to diffuse into deeper cell layers. Situation-dependent distinct cell deaths might be induced which could influence cell–cell-contacts and therefore the spheroid morphology. Consequently, differences in the induction of apoptosis and necrosis might be analyzed after spheroid treatment with non-PEGylated and PEGylated Cu(DDC)$_2$ liposomes. Particularly apoptosis leads to a dissolution of cellular binding properties [40]. The usage of light sheet fluorescence microscopy could give further information on the penetration behavior of fluorescence-labeled Cu(DDC)$_2$ liposomes in 3D spheroids [6,7]. Nonetheless, far higher EC$_{50}$ values were obtained as expected after Cu(DDC)$_2$ liposome treatment of 3D LS monoculture spheroids compared to those of 2D LS monolayers. Reasons for the drug resistance of 3D LS spheroids are obviously attributed to specific cellular interactions of the spheroid, to the three-dimensional arrangement of heterogeneous cell populations and the limited diffusion of mass transport which hinders the penetration of drugs and nanoparticles [6,7]. Moreover, cells of a spheroid are able to secrete components of an extracellular matrix (ECM) [3]. Desoize et al. (1998) described how cellular interactions with the microenvironment (cell–cell-contact and cell–ECM-contact) play a crucial role in resistance development against anticancer agents [41]. Presumably, a combination of the before mentioned factors leads to the resistance of 3D LS spheroids against Cu(DDC)$_2$ liposomes. Still, Cu(DDC)$_2$ liposomes effectively reduced the cell viability throughout different cell layers of the spheroid.

An effective drug candidate for cancer therapy should be able to reach the target tissue and to eliminate cancer cells without affecting non-malignant cells. Therefore, in the third part of this study the in vitro cytotoxicity of Cu(DDC)$_2$ liposomes on 2D primary cell models (hSkMC and hDFa) and 3D co-culture cell models (composed of neuroblastoma and primary cells) was analyzed. Here it was shown, that 2D hSkMC and 2D hDFa monolayers were less sensitive towards Cu(DDC)$_2$ liposomes compared to 2D LS monolayers. Likewise, Wehbe et al. (2016) observed in vitro a less cytotoxic effect of Cu(DDC)$_2$ liposomes on a primary cell line compared to cancer cells [8]. A possible explanation for the outcome could be a cell line-specific internalization rate for liposomes, since the uptake rate of nanoparticles was reported to be lower for non-malignant cells than for cancer cells [42,43]. Thus, the internalization rates of hSkMC and hDFa should be analyzed via uptake experiments similar to Section 3.2. Nevertheless, Cu(DDC)$_2$ liposomes turned out to reduce the

cell viability of primary cell lines, which means that healthy tissue could also be affected during efficient treatment of an in vivo tumor. This problem might be solved via surface modifications of liposomes with antibodies or antibody fragments to specifically target cancer cells [44]. For a more reliable evaluation of the cytotoxic efficiency of $Cu(DDC)_2$ liposomes and heterotypic 3D-LS-hSkMC and 3D-LS-hDFa co-culture spheroids were used as cell models. The achieved EC_{50} values of LS co-culture spheroids did not differ from those of LS monoculture spheroids. Furthermore, the same morphological changes of LS monoculture spheroids after treatment with $Cu(DDC)_2$ liposomes were observed for LS co-culture spheroids. It was expected, that hSkMC and/or hDFa eventually influence the spheroid resistance towards $Cu(DDC)_2$ liposomes, which was not observed in this study. In particular fibroblasts, as cancer associated fibroblasts (CAFs), have tumor-promoting effects, supporting the proliferation and metastasis of cancer cells and enhancing resistances against anticancer drugs [45]. Attention should be paid to the fact, that fibroblasts are a highly heterogeneous cell population with phenotypic characteristics, which strongly differ from where they originate [46]. It could be possible, that the hDFa used in this study were not suitable to mimic CAFs in 3D spheroids. Therefore, a combination of fibroblasts and myoblasts is suggested to be ideal for the generation of CAFs [47].

Further work is considered to be of interest for the future. This includes the transfer of the liposome preparation process from lab scale to large scale. Different preparation techniques, such as high pressure homogenization [48], microfluidization [49], cross flow filtration [50], or dual asymmetric centrifugation [51,52] can be implemented for the production of large volumes of Cu^{2+} liposomes. Formation of $Cu(DDC)_2$ complexes inside the liposomes and separation of non-encapsulated material may be achieved by using industrial high throughput columns and high pressure filtration under aseptic conditions.

Additional neuroblastoma cell lines might be of interest for further development and formation of 3D spheroids. Labeling of liposomal components and fluorescence activated cell sorting after incubation and later destruction of the spheroid might be helpful to gain more knowledge about the distribution and intraspheroidal processing of the liposomes and its contents in the different regions of the spheroid.

5. Conclusions

This study shows that the treatment of 3D spheroids, compared to 2D monolayers, provides more information concerning the cytotoxic effectiveness of $Cu(DDC)_2$ liposomes. Accordingly, it was proven that $Cu(DDC)_2$ liposomes effectively reduced the viability of in vitro neuroblastoma 3D spheroids. As it turned out that primary surrounding cells will also be affected, the implementation of a targeting structure on the nanocarriers seems to be of importance for reducing unwanted side effects and will, therefore, be in the focus of further studies.

References

1. López-Lázaro, M. Two Preclinical Tests to Evaluate Anticancer Activity and to Help Validate Drug Candidates for Clinical Trials. *Oncoscience* **2015**, *2*, 91–98. [CrossRef]
2. Edmondson, R.; Broglie, J.J.; Adcock, A.F.; Yang, L. Three-Dimensional Cell Culture Systems and Their Applications in Drug Discovery and Cell-Based Biosensors. *Assay Drug Dev. Technol.* **2014**, *12*, 207–218. [CrossRef]
3. Breslin, S.; O'Driscoll, L. Three-Dimensional Cell Culture: The Missing Link in Drug Discovery. *Drug Discov. Today* **2013**, *18*, 240–249. [CrossRef]
4. Nunes, A.S.; Barros, A.S.; Costa, E.C.; Moreira, A.F.; Correia, I.J. 3D Tumor Spheroids as in Vitro Models to Mimic in Vivo Human Solid Tumors Resistance to Therapeutic Drugs. *Biotechnol. Bioeng.* **2019**, *116*, 206–226. [CrossRef]
5. Lazzari, G.; Couvreur, P.; Mura, S. Multicellular Tumor Spheroids: A Relevant 3D Model for the in Vitro Preclinical Investigation of Polymer Nanomedicines. *Polym. Chem.* **2017**, *8*, 4947–4969. [CrossRef]
6. Tchoryk, A.; Taresco, V.; Argent, R.H.; Ashford, M.; Gellert, P.R.; Stolnik, S.; Grabowska, A.; Garnett, M.C. Penetration and Uptake of Nanoparticles in 3D Tumor Spheroids. *Bioconjug. Chem.* **2019**, *30*, 1371–1384. [CrossRef] [PubMed]
7. Yingchoncharoen, P.; Kalinowski, D.S.; Richardson, D.R. Lipid-Based Drug Delivery Systems in Cancer Therapy: What Is Available and What Is yet to Come. *Pharm. Rev.* **2016**, *68*, 701–787. [CrossRef]
8. Wehbe, M.; Anantha, M.; Backstrom, I.; Leung, A.; Chen, K.; Malhotra, A.; Edwards, K.; Bally, M.B. Nanoscale Reaction Vessels Designed for Synthesis of Copper-Drug Complexes Suitable for Preclinical Development. *PLoS ONE* **2016**, *11*, e0153416. [CrossRef] [PubMed]
9. Wehbe, M.; Anantha, M.; Shi, M.; Leung, A.W.; Dragowska, W.H.; Sanche, L.; Bally, M.B. Development and Optimization of an Injectable Formulation of Copper Diethyldithiocarbamate, an Active Anticancer Agent. *Int. J. Nanomed.* **2017**, *12*, 4129–4146. [CrossRef] [PubMed]
10. Johansson, B. A Review of the Pharmacokinetics and Pharmacodynamics of Disulfiram and Its Metabolites. *Acta Psychiatr. Scand. Suppl.* **1992**, *369*, 15–26. [CrossRef] [PubMed]
11. Rudolph, G.; Schilbach-Stückle, K.; Handgretinger, R.; Kaiser, P.; Hameister, H. Cytogenetic and Molecular Characterization of a Newly Established Neuroblastoma Cell Line LS. *Hum. Genet.* **1991**, *86*, 562–566. [CrossRef]
12. Colon, N.C.; Chung, D.H. Neuroblastoma. *Adv. Pediatr.* **2011**, *58*, 297–311. [CrossRef] [PubMed]
13. Davidoff, A.M. Neuroblastoma. *Semin Pediatr. Surg* **2012**, *21*, 2–14. [CrossRef] [PubMed]
14. Kholodenko, I.V.; Kalinovsky, D.V.; Doronin, I.I.; Deyev, S.M.; Kholodenko, R.V. Neuroblastoma Origin and Therapeutic Targets for Immunotherapy. Available online: https://www.hindawi.com/journals/jir/2018/7394268/ (accessed on 15 May 2020).
15. Maris, J.M. Recent Advances in Neuroblastoma. *N. Engl. J. Med.* **2010**, *362*, 2202–2211. [CrossRef]
16. Flahaut, M.; Jauquier, N.; Chevalier, N.; Nardou, K.; Balmas Bourloud, K.; Joseph, J.-M.; Barras, D.; Widmann, C.; Gross, N.; Renella, R.; et al. Aldehyde Dehydrogenase Activity Plays a Key Role in the Aggressive Phenotype of Neuroblastoma. *BMC Cancer* **2016**, *16*, 781. [CrossRef]
17. Chen, D.; Cui, Q.C.; Yang, H.; Dou, Q.P. Disulfiram, a Clinically Used Anti-Alcoholism Drug and Copper-Binding Agent, Induces Apoptotic Cell Death in Breast Cancer Cultures and Xenografts via Inhibition of the Proteasome Activity. *Cancer Res.* **2006**, *66*, 10425–10433. [CrossRef]
18. Butcher, K.; Kannappan, V.; Kilari, R.S.; Morris, M.R.; McConville, C.; Armesilla, A.L.; Wang, W. Investigation of the Key Chemical Structures Involved in the Anticancer Activity of Disulfiram in A549 Non-Small Cell Lung Cancer Cell Line. *BMC Cancer* **2018**, *18*, 753. [CrossRef]
19. Guo, F.; Yang, Z.; Kulbe, H.; Albers, A.E.; Sehouli, J.; Kaufmann, A.M. Inhibitory Effect on Ovarian Cancer ALDH+ Stem-like Cells by Disulfiram and Copper Treatment through ALDH and ROS Modulation. *Biomed. Pharm.* **2019**, *118*, 109371. [CrossRef] [PubMed]
20. Liu, P.; Brown, S.; Goktug, T.; Channathodiyil, P.; Kannappan, V.; Hugnot, J.-P.; Guichet, P.-O.; Bian, X.; Armesilla, A.L.; Darling, J.L.; et al. Cytotoxic Effect of Disulfiram/Copper on Human Glioblastoma Cell Lines and ALDH-Positive Cancer-Stem-like Cells. *Br. J. Cancer* **2012**, *107*, 1488–1497. [CrossRef]
21. Liu, P.; Kumar, I.S.; Brown, S.; Kannappan, V.; Tawari, P.E.; Tang, J.Z.; Jiang, W.; Armesilla, A.L.; Darling, J.L.; Wang, W. Disulfiram Targets Cancer Stem-like Cells and Reverses Resistance and Cross-Resistance in Acquired Paclitaxel-Resistant Triple-Negative Breast Cancer Cells. *Br. J. Cancer* **2013**, *109*, 1876–1885. [CrossRef] [PubMed]
22. Bangham, A.D.; Standish, M.M.; Watkins, J.C. Diffusion of Univalent Ions across the Lamellae of Swollen Phospholipids. *J. Mol. Biol.* **1965**, *13*, 238–252. [CrossRef]
23. Olson, F.; Hunt, C.A.; Szoka, F.C.; Vail, W.J.; Papahadjopoulos, D. Preparation of Liposomes of Defined Size Distribution by Extrusion through Polycarbonate Membranes. *Biochim. Biophys. Acta* **1979**, *557*, 9–23. [CrossRef]
24. Bartlett, G.R. Phosphorus Assay in Column Chromatography. *J. Biol. Chem.* **1959**, *234*, 466–468. [CrossRef]
25. Friedrich, J.; Seidel, C.; Ebner, R.; Kunz-Schughart, L.A. Spheroid-Based Drug Screen: Considerations and Practical Approach. *Nat. Protoc.* **2009**, *4*, 309–324. [CrossRef] [PubMed]
26. Kemmer, G.; Keller, S. Nonlinear Least-Squares Data Fitting in Excel Spreadsheets. *Nat. Protoc* **2010**, *5*, 267–281. [CrossRef]
27. Kolter, M.; Wittmann, M.; Köll-Weber, M.; Süss, R. The Suitability of Liposomes for the Delivery of Hydrophobic Drugs—A Case Study with Curcumin. *Eur. J. Pharm. Biopharm.* **2019**, *140*, 20–28. [CrossRef]

28. Sahlin, S.; Hed, J.; Rundquist, I. Differentiation between Attached and Ingested Immune Complexes by a Fluorescence Quenching Cytofluorometric Assay. *J. Immunol. Methods* **1983**, *60*, 115–124. [CrossRef]

29. Grit, M.; Crommelin, D.J. Chemical Stability of Liposomes: Implications for Their Physical Stability. *Chem. Phys. Lipids* **1993**, *64*, 3–18. [CrossRef]

30. du Plessis, J.; Ramachandran, C.; Weiner, N.; Müller, D.G. The Influence of Lipid Composition and Lamellarity of Liposomes on the Physical Stability of Liposomes upon Storage. *Int. J. Pharm.* **1996**, *127*, 273–278. [CrossRef]

31. Muppidi, K.; Pumerantz, A.S.; Wang, J.; Betageri, G. Development and Stability Studies of Novel Liposomal Vancomycin Formulations. *Isrn Pharm.* **2012**, *2012*, e636743. [CrossRef]

32. Stark, B.; Pabst, G.; Prassl, R. Long-Term Stability of Sterically Stabilized Liposomes by Freezing and Freeze-Drying: Effects of Cryoprotectants on Structure. *Eur. J. Pharm. Sci.* **2010**, *41*, 546–555. [CrossRef]

33. Ramana, L.N.; Sharma, S.; Sethuraman, S.; Ranga, U.; Krishnan, U.M. Investigation on the Stability of Saquinavir Loaded Liposomes: Implication on Stealth, Release Characteristics and Cytotoxicity. *Int. J. Pharm.* **2012**, *431*, 120–129. [CrossRef]

34. Sato, T.; Sakai, H.; Sou, K.; Buchner, R.; Tsuchida, E. Poly(Ethylene Glycol)-Conjugated Phospholipids in Aqueous Micellar Solutions: Hydration, Static Structure, and Interparticle Interactions. *J. Phys. Chem. B* **2007**, *111*, 1393–1401. [CrossRef]

35. Tsermentseli, S.K.; Kontogiannopoulos, K.N.; Papageorgiou, V.P.; Assimopoulou, A.N. Comparative Study of PEgylated and Conventional Liposomes as Carriers for Shikonin. *Fluids* **2018**, *3*, 36. [CrossRef]

36. Tawari, P.E.; Wang, Z.; Najlah, M.; Tsang, C.W.; Kannappan, V.; Liu, P.; McConville, C.; He, B.; Armesilla, A.L.; Wang, W. The Cytotoxic Mechanisms of Disulfiram and Copper(Ii) in Cancer Cells. *Toxicol. Res.* **2015**, *4*, 1439–1442. [CrossRef] [PubMed]

37. Zamaraeva, M.V.; Sabirov, R.Z.; Maeno, E.; Ando-Akatsuka, Y.; Bessonova, S.V.; Okada, Y. Cells Die with Increased Cytosolic ATP during Apoptosis: A Bioluminescence Study with Intracellular Luciferase. *Cell Death Differ.* **2005**, *12*, 1390–1397. [CrossRef] [PubMed]

38. Kostarelos, K.; Emfietzoglou, D.; Papakostas, A.; Yang, W.-H.; Ballangrud, A.; Sgouros, G. Binding and Interstitial Penetration of Liposomes within Avascular Tumor Spheroids. *Int. J. Cancer* **2004**, *112*, 713–721. [CrossRef] [PubMed]

39. Niora, M.; Pedersbaek, D.; Lassen, R.M.M.; de Val Weywadt, M.F.; Andresen, T.L.; Simonsen, J.B.; Jauffred, L. Head-to-Head Comparison of the Penetration Efficiency of Lipid-Based Nanoparticles in a 3D Tumor Spheroid Model. *Acs Omega* **2020**, *5*, 21162–21171. [CrossRef]

40. Steinhusen, U.; Weiske, J.; Badock, V.; Tauber, R.; Bommert, K.; Huber, O. Cleavage and Shedding of E-Cadherin after Induction of Apoptosis. *J. Biol. Chem.* **2001**, *276*, 4972–4980. [CrossRef] [PubMed]

41. Desoize, B.; Gimonet, D.; Jardillier, J.C. Multicellular resistance: Another mechanisms of pleiotropic resistance? *Bull. Cancer* **1998**, *85*, 785–793.

42. Huang, P.; Yang, C.; Liu, J.; Wang, W.; Guo, S.; Li, J.; Sun, Y.; Dong, H.; Deng, L.; Zhang, J.; et al. Improving the Oral Delivery Efficiency of Anticancer Drugs by Chitosan Coated Polycaprolactone-Grafted Hyaluronic Acid Nanoparticles. *J. Mater. Chem. B* **2014**, *2*, 4021–4033. [CrossRef]

43. Chaves, N.L.; Estrela-Lopis, I.; Böttner, J.; Lopes, C.A.; Guido, B.C.; de Sousa, A.R.; Báo, S.N. Exploring Cellular Uptake of Iron Oxide Nanoparticles Associated with Rhodium Citrate in Breast Cancer Cells. *Int. J. Nanomed.* **2017**, *12*, 5511–5523. [CrossRef]

44. Riaz, M.K.; Riaz, M.A.; Zhang, X.; Lin, C.; Wong, K.H.; Chen, X.; Zhang, G.; Lu, A.; Yang, Z. Surface Functionalization and Targeting Strategies of Liposomes in Solid Tumor Therapy: A Review. *Int. J. Mol. Sci.* **2018**, *19*, 195. [CrossRef] [PubMed]

45. Sahai, E.; Astsaturov, I.; Cukierman, E.; DeNardo, D.G.; Egeblad, M.; Evans, R.M.; Fearon, D.; Greten, F.R.; Hingorani, S.R.; Hunter, T.; et al. A Framework for Advancing Our Understanding of Cancer-Associated Fibroblasts. *Nat. Rev. Cancer* **2020**, *20*, 174–186. [CrossRef] [PubMed]

46. Chang, H.Y.; Chi, J.-T.; Dudoit, S.; Bondre, C.; van de Rijn, M.; Botstein, D.; Brown, P.O. Diversity, Topographic Differentiation, and Positional Memory in Human Fibroblasts. *Proc. Natl. Acad. Sci. USA* **2002**, *99*, 12877–12882. [CrossRef] [PubMed]

47. Kojima, Y.; Acar, A.; Eaton, E.N.; Mellody, K.T.; Scheel, C.; Ben-Porath, I.; Onder, T.T.; Wang, Z.C.; Richardson, A.L.; Weinberg, R.A.; et al. Autocrine TGF-Beta and Stromal Cell-Derived Factor-1 (SDF-1) Signaling Drives the Evolution of Tumor-Promoting Mammary Stromal Myofibroblasts. *Proc. Natl. Acad. Sci. USA* **2010**, *107*, 20009–20014. [CrossRef]

48. Brandl, M.; Drechsler, M.; Bachmann, D.; Tardi, C.; Schmidtgen, M.; Bauer, K.-H. Preparation and Characterization of Semi-Solid Phospholipid Dispersions and Dilutions Thereof. *Int. J. Pharm.* **1998**, *170*, 187–199. [CrossRef]

49. Jahn, A.; Vreeland, W.N.; DeVoe, D.L.; Locascio, L.E.; Gaitan, M. Microfluidic Directed Formation of Liposomes of Controlled Size. *Langmuir* **2007**, *23*, 6289–6293. [CrossRef]

50. Peschka, R.; Purmann, T.; Schubert, R. Cross-Flow Filtration—An Improved Detergent Removal Technique for the Preparation of Liposomes. *Int. J. Pharm.* **1998**, *162*, 177–183. [CrossRef]

51. Massing, U.; Cicko, S.; Ziroli, V. Dual Asymmetric Centrifugation (DAC)—A New Technique for Liposome Preparation. *J. Control. Release* **2008**, *125*, 16–24. [CrossRef]

52. Massing, U.; Ingebrigtsen, S.G.; Škalko-Basnet, N.; Holsæter, A.M. Dual Centrifugation—A Novel "in-vial" Liposome Processing Technique. In *Liposomes*; IntechOpen: Lundon, UK, 2017; Available online: https://www.intechopen.com/books/liposomes/dual-centrifugation-a-novel-in-vial-liposome-processing-technique (accessed on 25 March 2021).